Authors' submitted manuscript (preprint)
Article published in Industrial Crops and Products, Vol. 222, Part 4, 2024.
The final published version available at https://doi.org/10.1016/j.indcrop.2024.119883

Areca nut husk biochar as a sustainable carbonaceous filler for cement: Pyrolysis temperature and its effect on characterization, strength, and hydration

Balasubramanya Manjunath [1,4], Claudiane M. Ouellet-Plamondon [2], B B Das [3], Subba Rao [1], Chandrasekhar Bhojaraju [4*], Manu Rao [1*]

[1] Department of Water Resources and Ocean Engineering, National Institute of Technology Karnataka, Surathkal, India.

[2] Department of Construction Engineering, University of Quebec, École de technologie supérieure (ÉTS), 1100 Notre-Dame West, Montréal, QC, H3C 1K3, Canada.

[3] Department of Civil Engineering, National Institute of Technology Karnataka, Surathkal, India.

[4] Department of Civil Engineering, St. Joseph Engineering College, Vamanjoor, Mangaluru, Karnataka, India. 575028.

First author: manjunathb.217wo501@nitk.edu.in , manjunathb@sjec.ac.in

[*] Corresponding authors: manurao@nitk.edu.in , chandrasekhar.b@sjec.ac.in

Highlights

- Areca nut husk is a potential agro-waste for the preparation of biochar, offering a sustainable carbonaceous filler for cement.
- Increase in the pyrolysis temperature of areca nut husk biochar (AB) leads to a decrease in H/C and O/C, indicating the aromaticity of the biochar.
- Micro filler effect of AB improves the early strength of cement mortar.
- Degree of hydration is improved with the addition of AB, confirmed by Bhatty's method.
- AB reduced CO_2 equivalent emissions compared with cement mortar.

Graphical Abstract

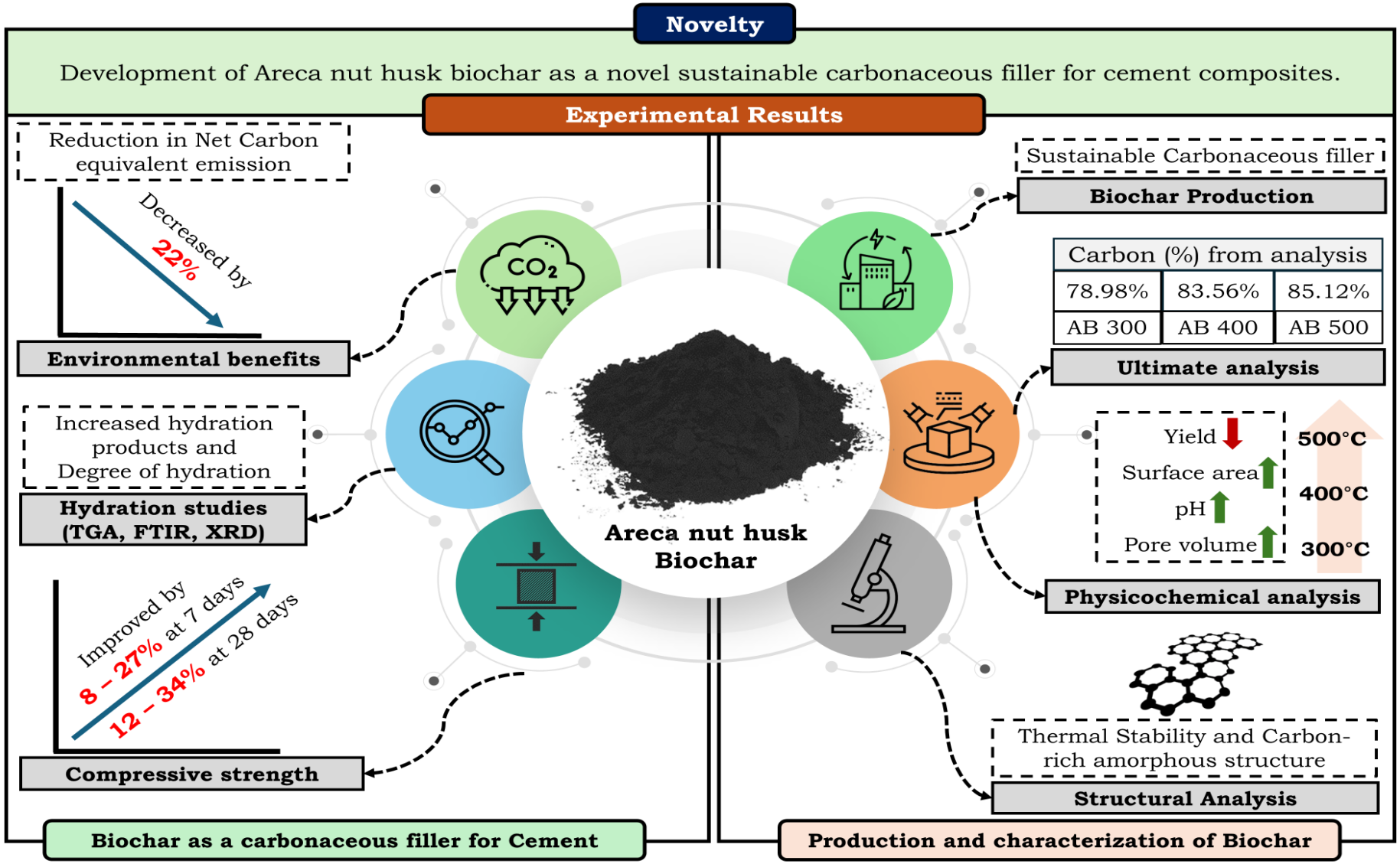

Abstract

This study addresses the gap in sustainable agro-based materials for cement by exploring locally available areca nut husk pyrolyzed into areca nut husk biochar (AB). The research investigated the effect of pyrolysis temperature (300°C, 400°C, and 500°C) on the characteristics of AB and its impact on cementitious performance. The study found that increasing pyrolysis temperatures led to lower yield, greater aromaticity, and increased surface area of AB. Fourier Transform Infrared Spectroscopy (FTIR) analysis showed decreased functional groups in AB at higher temperatures, confirming enhanced carbonization. Thermogravimetric analysis (TGA) revealed greater thermal stability of AB. X-ray diffraction (XRD) indicated a carbon-rich amorphous structure and crystalline graphite carbon formation in AB. Incorporating AB at 2% into cementitious composites substantially increased the compressive strength compared to the control mortar. At 7 and 28 days, the compressive strength increased by 8% and 12% for AB 300, 16% and 21% for AB 400, and 27% and 34% for AB 500. This improvement was due to the micro filler effect of AB, which improved the compactness of the cementitious matrix. Hydration studies from TGA showed that the addition of AB accelerated early-stage hydration, with the degree of hydration increasing from 46% (in control mix) to 48-53% in AB blended mixes using Bhatty's method. FTIR analysis demonstrated improved hydration of silicate phases and C-S-H formation in the presence of AB, supported by XRD analysis. AB blended mortar reduced the CO_2 equivalent emission by 22% compared to the control mortar attributed to its carbon sequestration capacity. These results highlight the potential of AB as a sustainable carbonaceous filler for cementitious composites, offering an environmentally friendly option for future research in construction materials.

Keywords: Areca nut husk biochar, Carbonaceous filler, Strength, Hydration, Sustainability

Authors' submitted manuscript (preprint)
Article published in Industrial Crops and Products, Vol. 222, Part 4, 2024.
The final published version available at https://doi.org/10.1016/j.indcrop.2024.119883

1. Introduction

The significant increase in global carbon dioxide (CO_2) emissions and other greenhouse gases (GHG) severely impacted the environment (Liu et al., 2019), leading to climate change and ecological imbalances. Anthropogenic activities threaten the ecosystems and stability of society, endangering the nation (Selvakumar et al., 2022). According to the Intergovernmental Panel on Climate Change (IPCC), by the end of the 21st century, atmospheric CO_2 concentrations will rise from 410 to 590 ppm, causing a potential global temperature to increase by 1.9°C (Marescaux et al., 2018). Numerous countries have set a goal to achieve carbon neutrality to counteract global warming. The European Union, China, and India have set targets for achieving carbon neutrality by 2050, 2060, and 2070. Several nations are implementing carbon emissions trading schemes based on market principles to incentivize a reduction in carbon dioxide emissions for those who surpass approved thresholds (Chen and Lin, 2021).

The construction sector is a significant contributor to GHG, accounting for approximately 40% of all energy CO_2 emissions (Rashid et al., 2024). Within this sector, the production of Portland cement is responsible for about 36% of the 7.7 gigatons of anthropogenic CO_2 emissions released globally by construction activities (Habert et al., 2020). This makes cement production the second-largest industrial source of CO_2 emissions worldwide, each ton releasing approximately 800 kg of CO_2 into the atmosphere (Andrew, 2018).

On the other hand, agricultural waste management presents a significant challenge due to its low recycling rate and substantial environmental impact. Agricultural activities generate approximately 1 billion tons of waste annually, contributing to about one-fifth of total GHG worldwide (Karić et al., 2022). In India, the Indian Council of Agricultural Research reports an annual generation of around 350 million tons per year (Thakur et al., 2020), which is expected to rise due to population growth (Lee et al., 2022). The current disposal methods, such as landfilling or incineration, account for 3% of global GHG emissions (Khan et al., 2021). The uncontrolled burning of agricultural waste further poses environmental concerns. Given these challenges, there is an urgent need to develop sustainable management practices for agricultural waste. Consequently, researchers are increasingly focusing on innovative approaches to reuse this waste, particularly in the development of green and low-carbon construction materials.

Carbon sequestration in cement-based materials offers an effective strategy to reduce CO_2 emissions in the construction industry (Javed et al., 2022). All agricultural wastes with high residual carbon content and low cost can be used to convert into porous carbon materials,

called biochar (Kim et al., 2023; Zhang et al., 2020). In this context, biochar emerges as an innovative solution to address environmental pollution and global warming, owing to its unique physicochemical properties and diverse applications. Biochar is a carbon-rich aromatic substance derived from biomass through thermochemical conversion under oxygen-limited conditions (Lehmann et al., 2011). Biochar acts as a carbon sequestration agent in various applications such as soil amendment, soil health, nutrient retention, soil pH, energy production, and building material. The IPCC reports biochar as a promising strategy to promote carbon neutrality, as one ton of biochar can sequester up to 2.6 tons of CO_2 (Azzi et al., 2019). Furthermore, biochar produced from biomass shows significant potential in the development of sustainable carbon materials (Yu et al., 2022). The production and characteristics of biochar are influenced by various factors illustrated in Fig. 1.

Several studies have explored the potential of storing and fixing carbon in soil with biochar. The properties of biochar are beneficial for both soil amendment and construction purposes. The addition of biochar into cement reduces the landfill demand, prevents the burning of waste, and promotes waste utilization (Sirico et al., 2021). Incorporating 1 kg of biochar into concrete can sequester approximately 2.5kg of CO_2 emissions (Dixit et al., 2021). The addition of biochar to cementitious mixtures is a promising attribute as a green admixture, making it an ideal option for concrete applications. Recent studies have demonstrated that biochar in cementitious materials can significantly enhance mechanical properties. Biochar produced at lower temperatures (300°C - 500°C) generally showed optimal results, as evidenced by mixed wood sawdust pyrolyzed at 300°C (2% replacement), improving early compressive strength (Gupta et al., 2018c), while in another study, biochar prepared with sawdust at 500°C showed a 45% improvement in strength (Ali et al., 2023). Further, waste wood biochar pyrolyzed at 400°C and 500°C (1 – 3% replacement) increased the strength by 25% (Tan et al., 2020a). Wood-based biochar proved to be very effective with pre-soaked wood sawdust (2% replacement) exhibiting an increase in compressive strength results by 40 – 50% (Gupta and Kua, 2018). The performance of biochar is significantly influenced by its source material, and agricultural waste-derived biochar has demonstrated promising results. Rice husk and bagasse biochar produced at 700°C (5% replacement) increased compressive strength by 36% and 55%, respectively (Zeidabadi et al., 2018). Olive-derived biochar has shown potential, with olive stone biochar (4% replacement) slightly improving compressive strength (Maljaee et al., 2021b) and olive tree pruning biochar at 5% replacement, resulting in a 13% improvement in strength (Kalderis et al., 2024). Other agricultural wastes like coconut, peanut, and wheat husk biochar (Javed et al., 2022), and junglee keekar (Rashid et al., 2024) at 2% and

5% of the cement replacement enhanced the strength. Industrial and municipal waste biochar have also been explored, with pulp and paper mill sludge biochar at 0.1% replacement providing similar strength to the control specimen (Akhtar and Sarmah, 2018). Nano-biochar from municipal solid waste at 0.12% replacement improved strength by 17% (Sisman et al., 2024). Various studies have shown that accelerated carbonation curing for biochar improved the mechanical properties of cementitious composites irrespective of the feedstock used (Kua and Tan, 2023; Yang and Wang, 2021). The optimal biochar dosage varies across studies but generally falls within the range of 1-5% by weight of cement. These comprehensive findings of biochar from diverse sources, along with different application methods, pyrolysis temperature, residence time, and quantity, exhibit biochar's significant potential in developing sustainable construction materials.

While existing research has explored a wide range of feedstocks for biochar preparation, there remains unexplored potential in other agricultural wastes. Notably, the use of areca nut husk biochar (AB) in construction applications represents a novel approach that has not been previously explored in the literature. This study aims to discover new avenues for sustainable construction practices by investigating the effects of AB as a sustainable carbonaceous filler in cementitious composites. The utilization of AB adds to the diversity of biochar sources and offers region-specific solutions, particularly in areas where areca nut waste is abundant. This novel application of AB in construction materials emphasizes the ongoing investigation in the field and the continuous efforts to find sustainable alternatives in the construction industry.

Areca nut, or betel nut, is a fruit of areca catechu palm species grown extensively in Southeast Asian countries (Bera and Mohanty, 2020). India is the world's largest producer of areca nut, with approximately 904 tons, with the majority of production occurring in Karnataka (Hugar et al., 2023). The areca nut husk is a lignocellulosic biomass that constitutes about 65 – 80 % of the total weight of the fruit (Vikraman et al., 2022). The areca nut is covered by a fibrous husk, discarded as agricultural waste with an estimated around 6 to 7 tons of waste available from 1 ha of areca nut plantation yearly, and has no market value. Improper disposal techniques of areca husks have led to significant environmental problems (Anuar et al., 2021). It undergoes slow decomposition and, therefore, cannot be used as manure. Fig. 2 shows the areca nut dumped (DHNS, 2020).

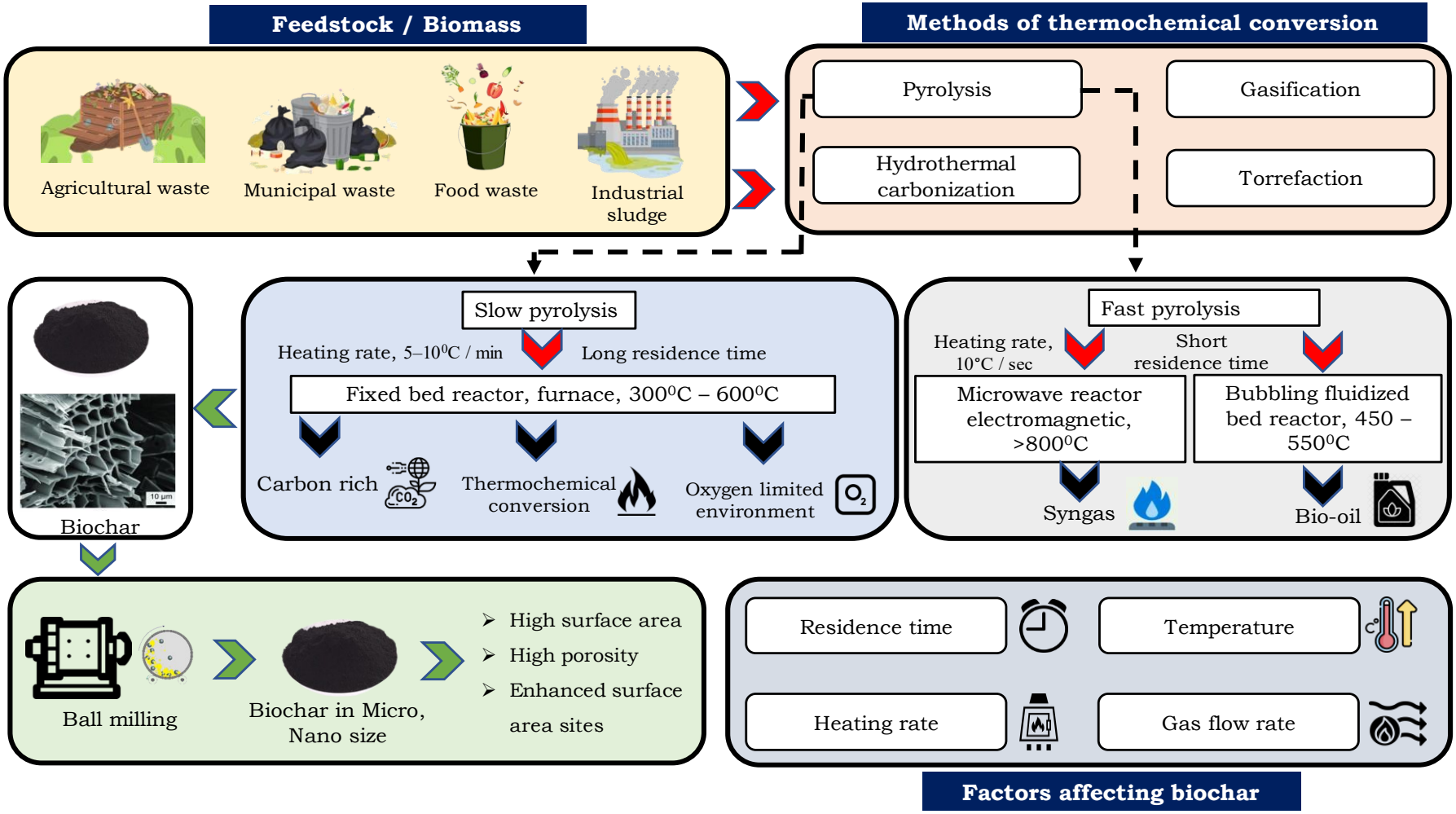

Fig. 1. Different feedstocks and methods to produce biochar

Fig. 2. Arecanut husk dumped

Few studies have shown that AB has the potential to remove heavy metals and soil amendment, improve fuel properties, and act as an adsorption agent. However, its use as a building material is still in its early stages. Hence, this study introduces an AB to the scientific community, expanding upon the conventional biochar utilized in cementitious composites. Further investigation and verification of the utilization of AB in engineering applications are needed to promote its wider adoption as a building material. The objectives of the present study are as follows:

1. To investigate the in-depth characteristics of novel green AB at different pyrolysis temperatures.
2. To determine the feasibility of AB as a sustainable carbonaceous filler in cementitious composites.

The present study carried out a comprehensive experimental program to achieve these objectives. Proximate analysis, ultimate analysis, physicochemical analysis, surface analysis, and structural analysis are carried out to investigate the characteristics of novel AB. Compressive strength, ultrasonic pulse velocity (UPV), and hydration studies such as X-ray diffraction (XRD), thermogravimetric analysis (TGA), and Fourier transform infrared spectroscopy (FTIR) were conducted.

2. Materials and Methods

2.1 Raw ingredients used

Ordinary Portland Cement (OPC) of grade 53 manufactured from UltraTech Cement Pvt. Ltd was used for all experimental work. The chemical composition and physical properties of the cement are presented in Table 1 and Table S1. The particle size distribution of the OPC was determined using a laser diffraction particle size analyzer, as shown in Fig. 3. The D10, D50, and D90 values of OPC are 3.12 µm, 22.49µm, and 57.80 µm, with the mean particle size of 27.40 µm. The specific surface area of OPC is 0.34 m^2/g. This study used locally available natural river sand as fine aggregates. The sand was washed to remove fine substances, sun-dried, sieved, and graded. The particle size curve for river sand (Fig. 3) confirms zone – II. The fine aggregate has a specific gravity of 2.68. The physical properties of sand are summarized in Table S2. Potable tap water was used to maintain the required moisture content during the casting and curing stages.

Table 1 Chemical composition of OPC

Chemical Composition (%)	SiO_2	CaO	Al_2O_3	Fe_2O_3	MgO	SO_3	K_2O	Na_2O	LOI
	18.59	63.87	6.22	4.98	1.54	3.24	0.25	0.2	0.98

2.2 Biochar Production

Areca nut husk, from the matured outer cover of an areca nut, was procured from Mangaluru, Karnataka, and was subjected to sun drying before further processing. The husks were then dried in the oven at 100°C for 24 h. The dried husks are further processed by mechanically reducing the size of the husk in a ball mill for 1 h and kept in the desiccator before being used to produce biochar.

Fig. S1 shows a programmable retort furnace used to produce biochar. The samples were subjected to pyrolysis at three different temperatures - 300°C, 400°C, and 500°C with a heating rate of 10°C / min and 1 h residence time. The furnace was purged with nitrogen gas to eliminate volatile products and ensure an oxygen-free atmosphere. The biochar produced by pyrolysis is shown in Fig. 4. The produced biochar was allowed to cool down to room temperature in a nitrogen environment. Fig. 5 shows the areca nut husk and the produced AB. The solid biochar remaining in the furnace was weighed and ground to a finer size for 3 min in a mixer grinder to AB and stored in the desiccator for characterization.

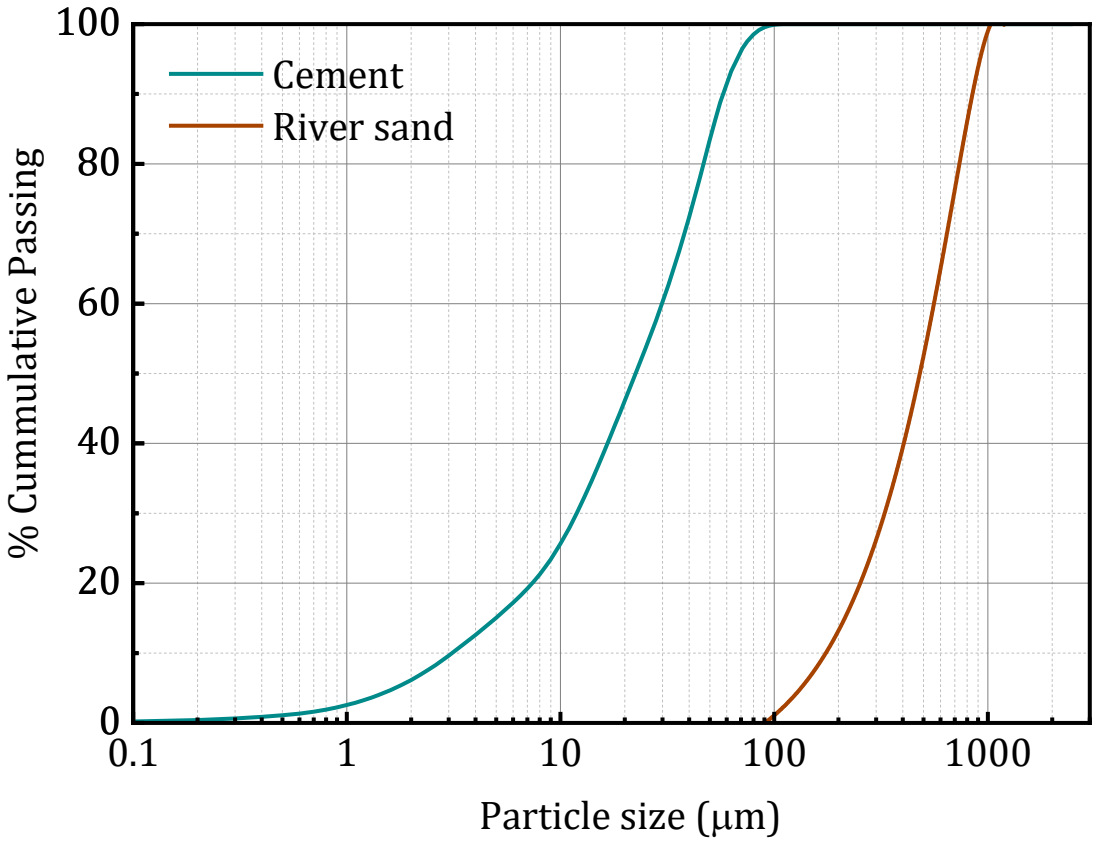

Fig. 3. Particle size distribution of raw materials

2.3 Characterization of biochar

The characterization techniques used for the produced AB are shown in Fig. 6.

2.3.1 Proximate analysis

Proximate analysis was conducted to assess critical parameters in AB, including moisture content (MC), volatile matter (VM), ash content (AC), and fixed carbon (FC), following ASTM E871-72, ASTM E872-82, and ASTM D1102-84, respectively. The comprehensive results of the proximate analysis are presented and discussed in section 3.

2.3.2 Ultimate analysis

The ultimate analysis of AB was performed to determine the percentages of Carbon (C), Hydrogen (H), Sulphur (S), Nitrogen (N), and Oxygen (O). The elemental model vario EL III elemental analyzer employs helium as a carrier gas combusted with approximately 10 mg of AB at 1100°C. The resulting gases (CO_2, H_2O, NO_2) were then transported to a detector to quantify the percentages of each element.

2.3.3 Physico-chemical analysis

The specific surface area, pore size, and pore volume of AB were determined using BET (Brunauer-Emmet-Teller) N_2 adsorption on the Autosorb IQ instrument by Anton Paar. Approximately 50 mg of AB was degassed for 8 h at 105°C. Particle size and zeta potential

were measured using dynamic light scattering (DLS) (Gujre et al., 2022) with the Lifesize 500 instrument. To determine pH values, AB samples were added to de-ionized water in a 1:20 mass ratio, followed by manually agitating and allowed to settle for 5 min before measuring with a pH meter (Gogoi et al., 2017). The same suspension is used to determine electrical conductivity using a conductivity meter.

2.3.4 Surface analysis

The surface morphology of AB samples was examined using a scanning electron microscope (SEM) (Joel, Japan).

2.3.5 Structural analysis

Crystalline phases present in AB were studied using XRD. The samples were scanned in the 2Θ range of 5 - 80° at a scan speed of 0.02°/s, from which qualitative information is extracted and analyzed. TGA characterizes the phase composition of the cement paste (Bhojaraju et al., 2021). TGA was performed on AB samples using a PerkinElmer thermal analyzer (TGA 4000). The weight loss was then monitored from 25 to 900°C, with a heating rate of 10°C / min under a protective nitrogen atmosphere. For FTIR analysis, the samples of AB were mixed with KBr, and these samples were then made into pellets using a pelletizer. The resulting pellets were placed in an FTIR instrument (PerkinElmer), which functioned from 600 to 4000 cm^{-1} to analyze the chemical groups contained in the samples.

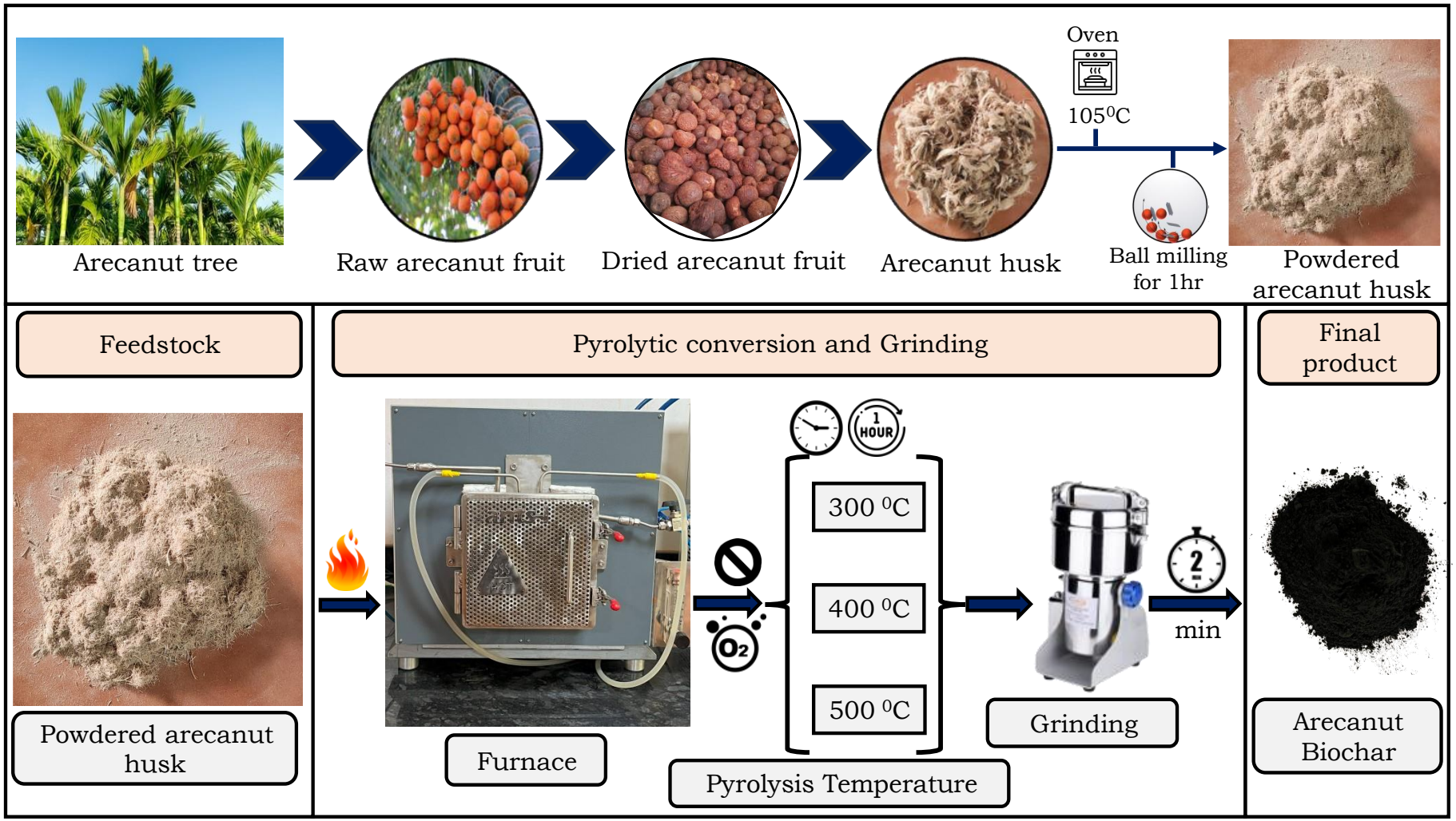

Fig. 4. Process used for the production of AB

231

Fig. 5. a) Dried areca nut husk – Before pyrolysis b) AB – After pyrolysis

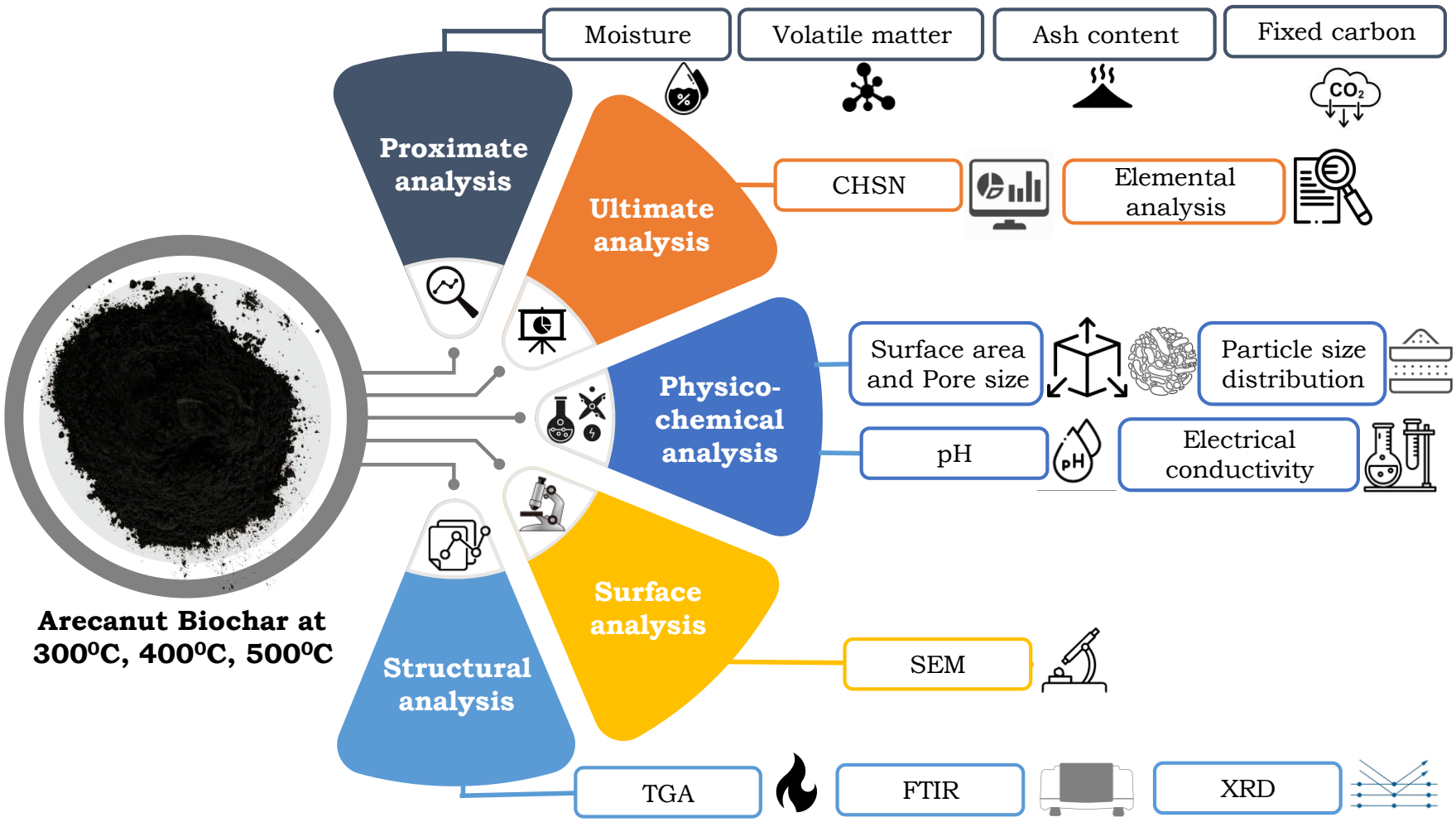

Fig. 6. Characterization techniques to determine the properties of biochar

2.4 Mix proportion and specimen preparation

The mortar was prepared with a proportion of 1:2.5:0.40 by weight of cement, sand, and water. The AB was mixed into cementitious composites at 2% by weight. The details of the mix proportions are shown in Table 2. The dry materials were mixed manually, and then the mixing water was added to the dry mixture. To attain homogeneity, all the materials are mixed at low speed for 1 min and 30 sec at high speed, and the mortar is left to rest for 90 sec to clean the sides of the bowl. The material is mixed for 1 min at high speed (Manjunath et al., 2023). After mixing, the fresh mixture was poured into the steel moulds with a cube size of 50 mm. The cubes were covered with polythene sheets for 24 h before being demoulded and then immersed in water for 7 and 28 days of curing.

Table 2 Mix proportions of paste and mortar samples

Mixes	OPC (g)	AB (g)	Water (g)	Sand (g)
PC	400	-	160	1000
AB 300	392	8	160	1000
AB 400	392	8	160	1000
AB 500	392	8	160	1000

2.5 Experimental methods

The study tested compressive strength tests on both control cement and AB-blended cement mortar at 7 and 28 days as per ASTM C-109. Three samples of each mix were tested for compressive strength, and mean values were plotted. UPV is also conducted to ascertain the quality and homogeneity of the mortar mixes as per ASTM C-597. Samples for XRD, TGA, and FTIR tests were obtained from the crushed cement pastes of 7 days curing age and ground to below 75 μm using a mortar pestle. All the samples were treated with isopropanol and diethyl ether to stop the hydration process.

3. Results and Discussions

3.1 Characterization of AB

3.1.1 Yield, Proximate analysis, Ultimate analysis of AB

Table 3 illustrates the significant impact of pyrolysis temperature on the properties of AB. As the pyrolysis temperature increases, the yield of AB decreases due to the volatilization of organic constituents in biomass. This results in a yield drop from 49 to 32%, as shown in Table 3. The proximate analysis reveals that increasing the pyrolysis temperature reduces the MC of AB samples due to carbonization (Elnour et al., 2019). Furthermore, the AC and FC of

all the AB samples increase with higher temperatures (Ross et al., 2008). The ultimate analysis demonstrates that carbonization increases the amount of C while decreasing the N, H, S, and O (by difference). The atomic ratios (H/C) and (O/C) for the AB samples ranged from 0.024 to 0.014 and 0.20 to 0.14, respectively. These changes indicate greater biomass pyrolysis and less hydrophilic AB surfaces at high temperatures (Elnour et al., 2019). These ratios suggest that all the AB samples fall within type IV on the Van Krevelen diagram (Ollivier et al., 2022), indicating significant aromaticity and high stability of AB

. The observed changes in ultimate analysis and atomic ratios reflect the formation of aromatic and graphitic structures, which can influence the interface interactions between filler and matrix (Elnour et al., 2019).

3.1.2 Physicochemical analysis of AB

The surface area and pore volume of biochar are critical quality indicators, significantly influencing the mechanical interlocking between filler and matrix. As shown in Table 4, increasing pyrolysis temperature leads to substantial improvement in both surface area and pore volume. The surface area increased from 4.34 to 112.38 m^2/g, while the pore volume improved from 0.006 to 0.07 cm^3/g. This enhancement is attributed to the elevated temperatures facilitating the release of volatile organic compounds and water, resulting in a more porous structure with a greater surface area (Yuan et al., 2015).

Fig. 7 presents the particle size distribution of all the AB samples, and the results are presented in Table 4. The size of AB is determined by DLS in the following order: AB 300 > AB 400 > AB 500. Compared to AB 300, the D50 and D90 of AB 400 and AB 500 are 22 – 45% and 38-88% finer, respectively. The size reduction is due to the increased pyrolysis temperature, resulting in a material breakdown and producing finer particles (Wang et al., 2013). The utilization of fine biochar enhances packing density and composite performance by effectively filling microscopic pores (Kua, 2024).

The zeta potential measurement evaluates the surface charge of particles and is shown in Table 4. The results indicate that the zeta potential of AB decreases with increasing pyrolysis temperature. This negative zeta potential generates a strong repulsive force between similarly charged particles, effectively mitigating particle aggregation and enhancing dispersion stability (Tan et al., 2020b).

The pH of biochar is significantly influenced by both feedstock type and pyrolysis temperature. The pH value of AB increases from 9.14 to 10.29, with increasing pyrolysis temperature, indicating an alkaline nature. This pH increase is primarily due to the removal of alkali salts from organic materials at higher pyrolysis temperatures (Wang et al., 2013).

The salinity of the biochar samples can be assessed by measuring the conductivity of the solution (Gujre et al., 2022). The results presented in Table 4 indicate that the electrical conductivity of AB increases with an increase in pyrolysis temperature, varying from 2.33 to 3.94 mS/cm. These findings agree with the previous studies (Gogoi et al., 2017), and are due to the increased ash concentration resulting from the loss of volatile matter during pyrolysis (Singh et al., 2017).

3.1.3 Surface Analysis of AB

Fig. 8 illustrates the morphology of AB particles and surface pores produced at 300°C, 400°C, and 500°C. SEM analysis reveals that all AB particles exhibit ridges and oval-shaped honeycomb pore structures on their surfaces (circled in yellow), reflecting the biological capillary structure of the areca nut husk feedstock. The pores of varying sizes are formed due to the release of volatiles and organic matter during pyrolysis (Gupta et al., 2018b). AB prepared at 500°C demonstrates more closely spaced pores compared to those prepared at 300°C and 400°C. The ridges on the AB surface enhance surface roughness, potentially leading to stronger bonding with the cementitious matrix (Gupta et al., 2018a). These pores serve a dual function, absorbing water and facilitating internal curing by releasing water during the hardening stage.

312 **Table 3** Chemical characteristics of biochar samples

Sample	Yield (%)	Proximate Analysis (%)				Ultimate analysis (%)					Atomic ratios	
		MC	VM	AC	FC	C	H	S	N	O (By difference)	H/C	O/C
AB 300	49	4.61	16.25	4.25	74.89	78.98	1.91	2.23	0.84	16.04	0.024	0.20
AB 400	39	3.21	14.89	5.98	75.92	83.56	1.65	1.00	0.19	13.60	0.019	0.16
AB 500	32	2.46	12.66	6.52	78.36	85.12	1.20	0.85	0.14	12.69	0.014	0.14

313 **Table 4** Physical characteristics of biochar samples

Sample	Particle Size (nm)			pH	Conductivity (mS/cm)	Surface area (m^2/g)	Total pore volume (cm^3/g)	Mean pore radius (nm)	Mean zeta potential (mV)
	D10	D50	D90						
AB 300	300	1418	12601	9.14	2.33	4.34	0.006	3.01	-19.59
AB 400	185	1113	1934	9.89	2.87	44.07	0.03	1.32	-11.38
AB 500	181	783	1444	10.29	3.94	112.38	0.07	1.29	-9.64

314

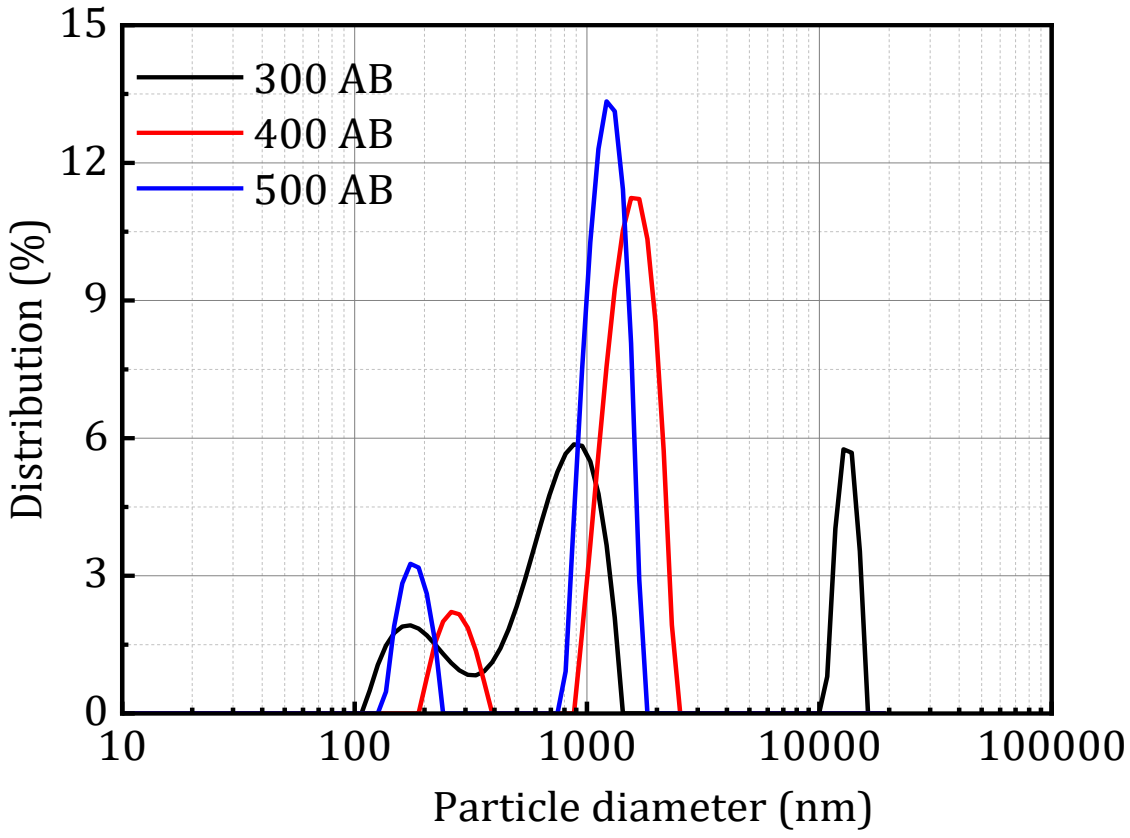

Fig. 7. Particle size distribution of AB

315

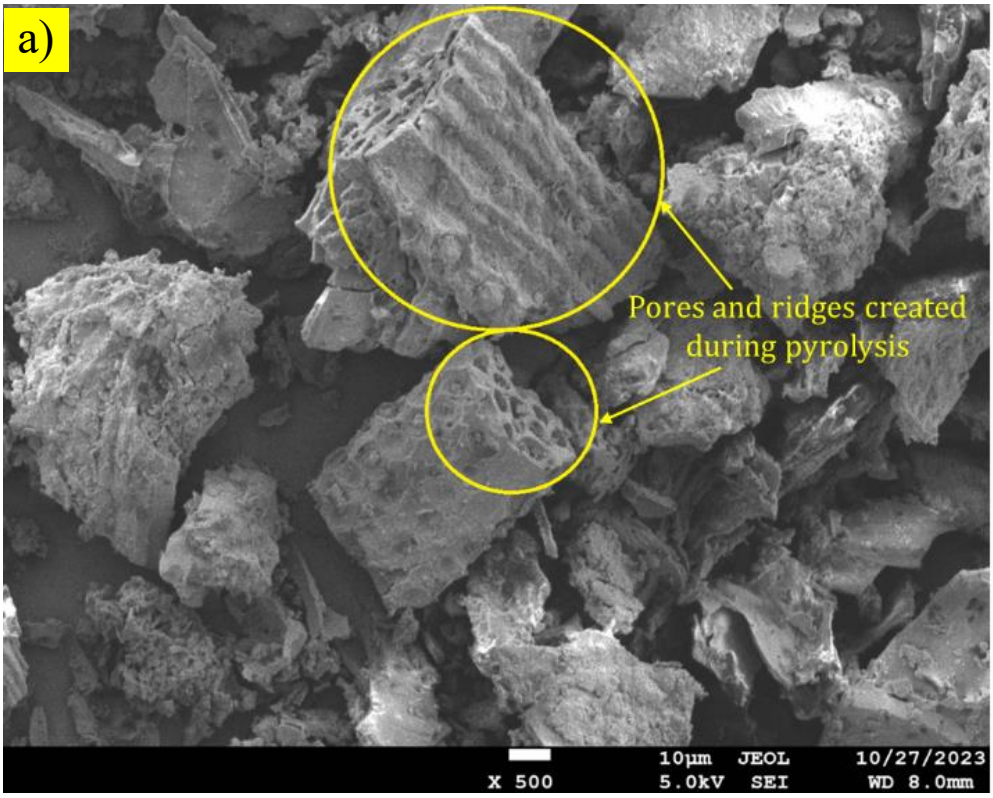

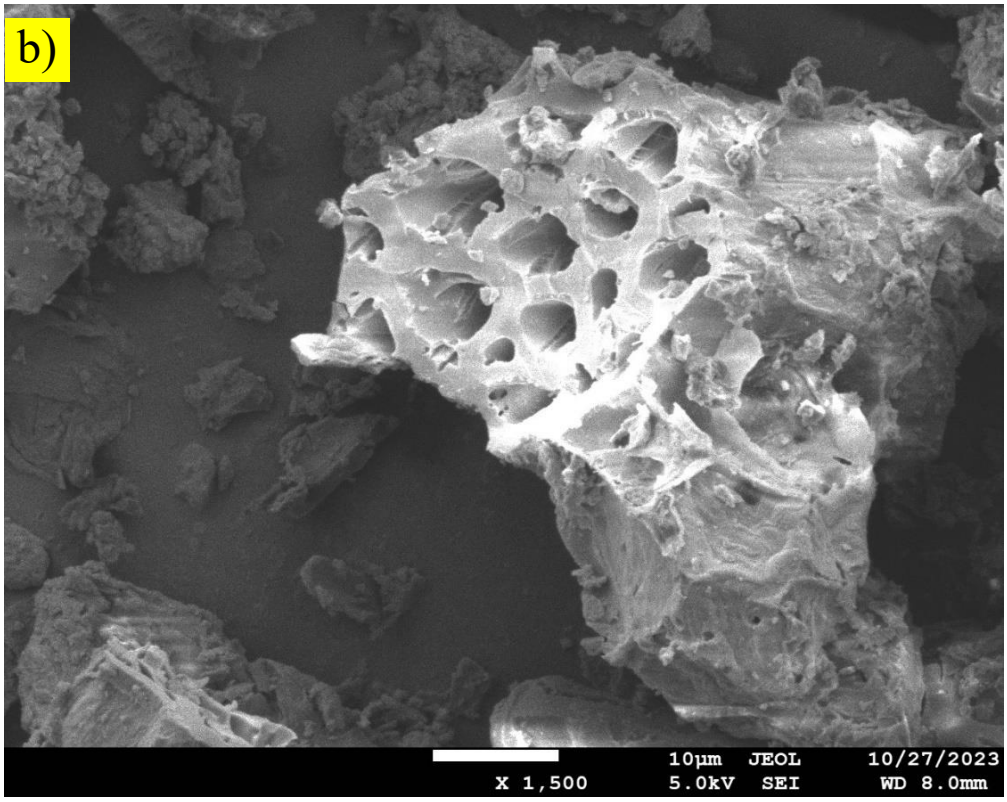
b)
X 1,500
10µm JEOL
5.0kV SEI
10/27/2023
WD 8.0mm

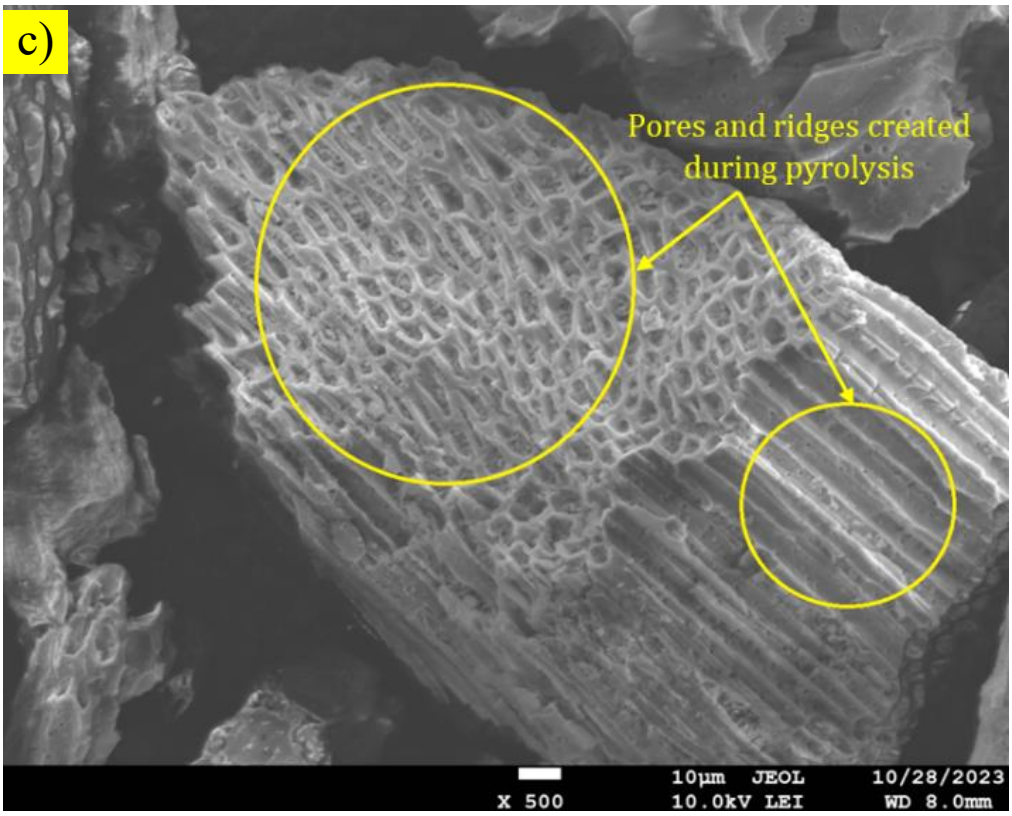
c)
Pores and ridges created
during pyrolysis
X 500
10µm JEOL
10.0kV LEI
10/28/2023
WD 8.0mm

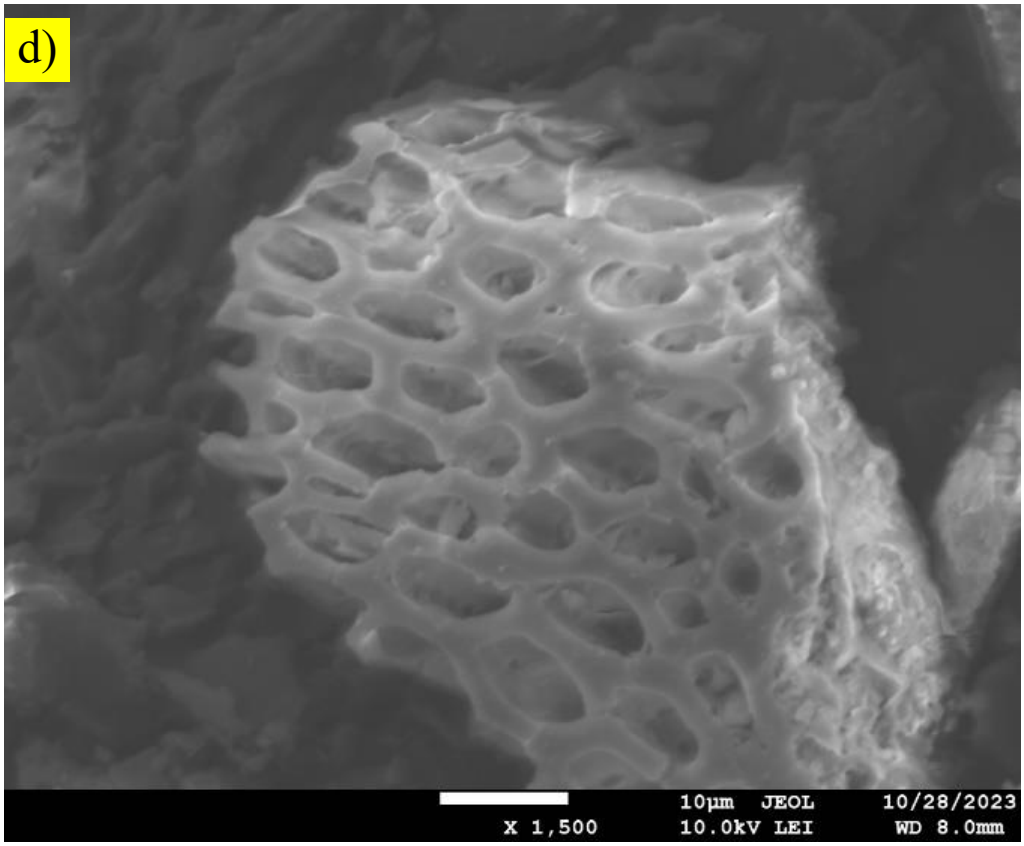
d)
10µm JEOL 10/28/2023
X 1,500 10.0kV LEI WD 8.0mm

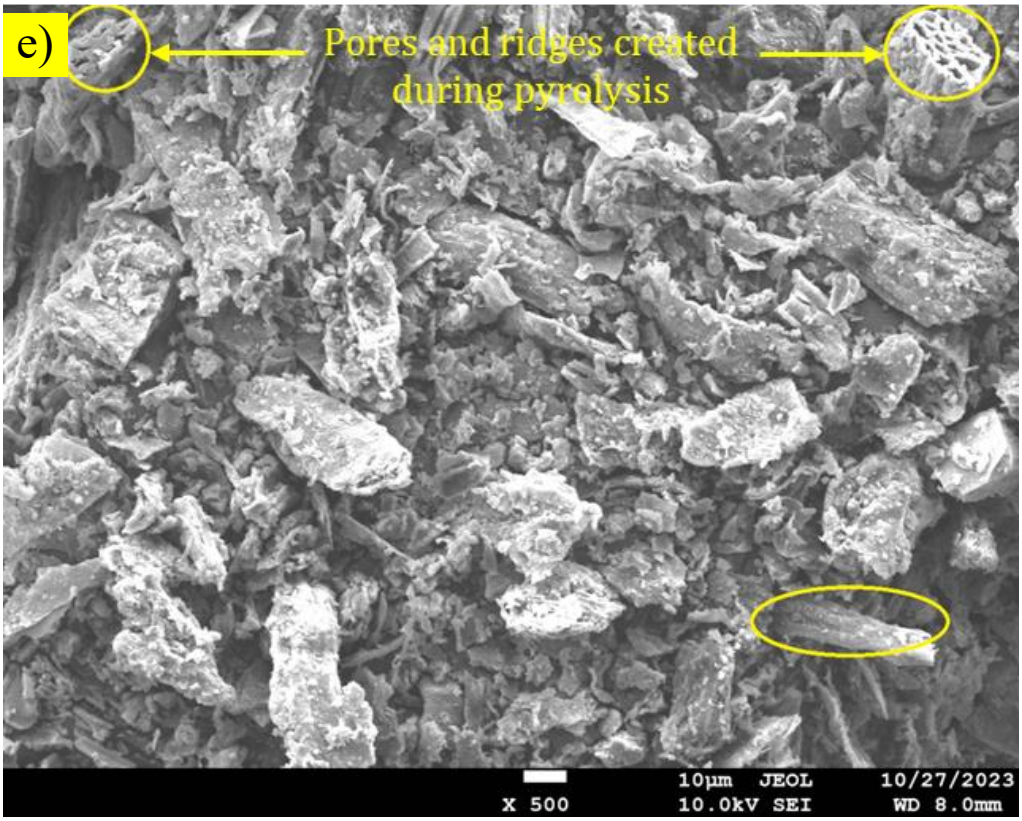
e)
Pores and ridges created during pyrolysis
10µm JEOL 10/27/2023
X 500 10.0kV SEI WD 8.0mm

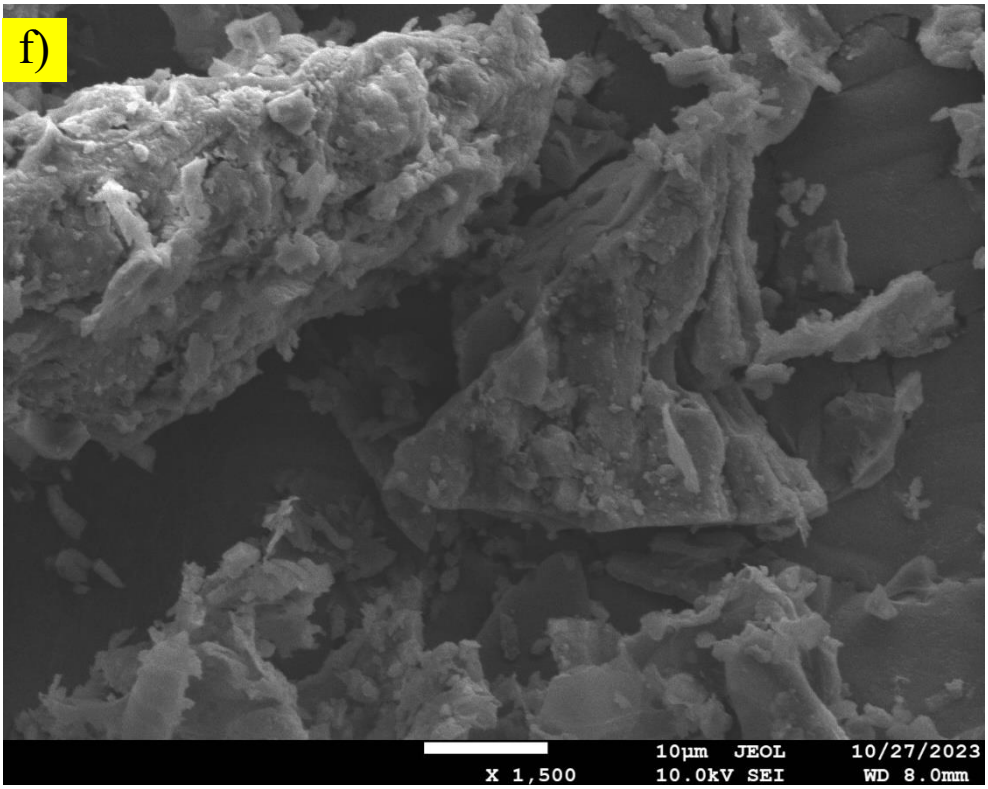

Fig. 8. SEM images of magnifications 500X and 1500X: a) and b) AB 300, c) and d) AB 400, e) and f) AB 500

3.1.4 Structural Analysis of AB

The thermal behaviour of AB prepared at different temperatures is studied using TGA and derivative thermogravimetry (DTG) curves. Fig. 9 shows that AB 300 experienced the highest weight loss (44%), followed by AB 400 (36%) and AB 500 (28%), with decreased weight loss at higher temperatures attributed to dehydrogenation, aromatization, and inorganic element degradation (Reza et al., 2020). The DTG curves present two prominent peaks for all AB samples. The first thermal peak phase occurs between 25 - 150°C for AB 300 and 25-200°C for AB 400 and AB 500, primarily results from moisture removal due to the hygroscopic nature of the biomass, resulting in the removal of moisture from its surface and pores (Pariyar et al., 2020). The second thermal peak phase observed between 150-650°C for AB 300 and 200-900°C for AB 400 and AB 500 corresponds to the degradation of hemicellulose, cellulose, and the gradual breakdown of lignin (Patwa et al., 2022). As pyrolysis temperature increased, the peaks for AB 400 and AB 500 shifted towards higher pyrolysis temperatures, with a significant reduction in peak height, suggesting the formation of more thermostable functional groups (Li and Chen, 2018). Similar results were observed for bamboo waste-derived biochar (Zhang et al., 2022). The thermal stability of AB prepared at higher temperatures agrees with the lower

atomic ratios. Table 5 presents the weight loss for various phases of the AB samples, providing an overview of the thermal degradation behaviour of AB.

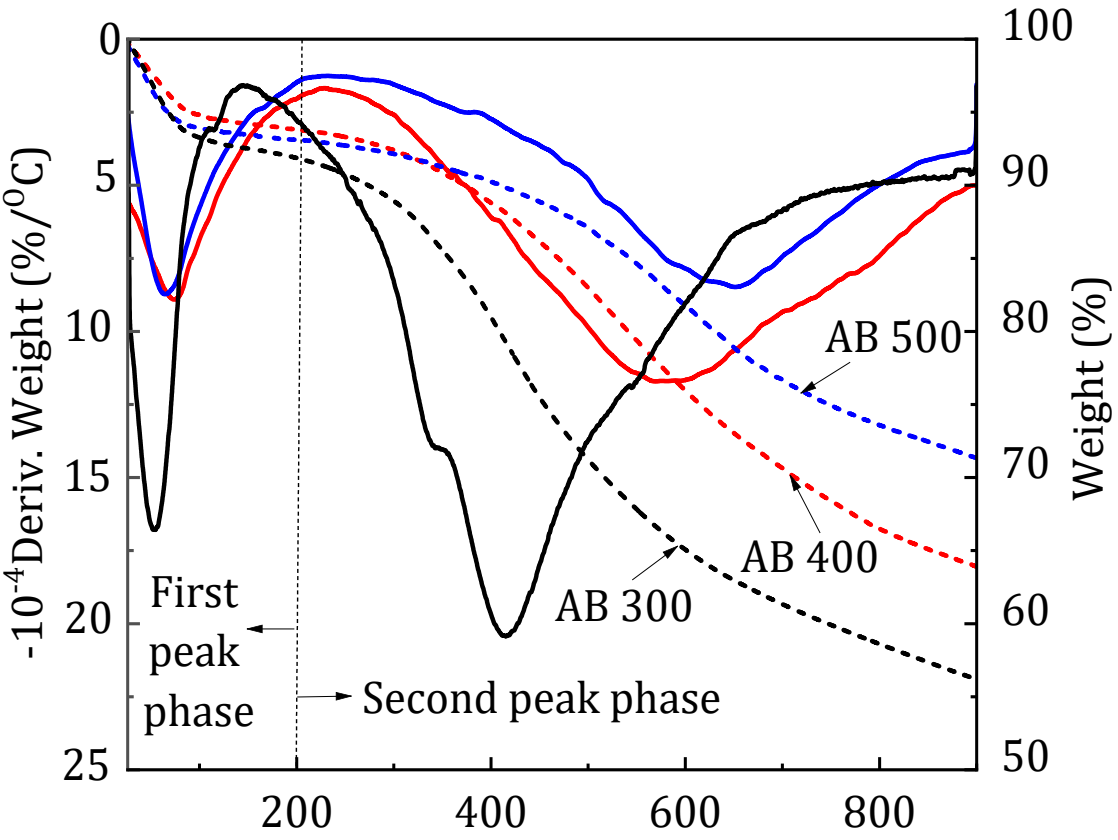

Fig. 9. TGA of AB

Table 5 Various phases of the TGA and DTG for AB with weight loss

Biochar	Weight loss for stage 1 (%)	Weight loss for stage 2 (%)	Residue (%)
AB 300	7.48	39.27	53.23
AB 400	6.21	31.87	61.91
AB 500	6.89	23.39	69.71

Fig. 10 presents the FTIR spectra of AB produced at various temperatures. The analysis shows that the functional groups are decreased with increasing pyrolysis temperatures due to enhanced carbonization and removal of volatile matter (Rafiq et al., 2016). A peak at 3388 cm^{-1} in the FTIR spectra corresponds to the O-H bond stretching of phenolic hydroxyl groups, which decreases at higher temperatures due to the loss of hydrogen and oxygen (Elnour et al., 2019). The C-H stretching vibration at 2870 cm^{-1} indicates the presence of cellulose, hemicellulose, and lignin. The peak decreases significantly as aliphatic structures transform into aromatic structures. Carbonyl bond (C=O) stretching vibration at 1710 cm^{-1} is associated with ketones and esters (Cantrell et al., 2012). An absorption band at 1594 cm^{-1} confirms

phenolic groups common in lignin and aromatic compounds, indicative of double bonded hydrocarbons (C=C) stretching vibrations (Sharma et al., 2004). The band at 1110 cm^{-1} corresponds to C-O-C groups in carbonyl derivatives. The absorbance at 770 cm^{-1} indicates aromatic C-H deformation, which is more prominent at higher temperatures (Kloss et al., 2012). The formation of graphite-like polyaromatic structures at higher temperatures results in less intense peaks (Bardalai and Mahanta, 2018). Overall, AB prepared at higher temperatures exhibits lower (H/C) and (O/C) ratios, indicating fewer surface functional groups and higher carbon content.

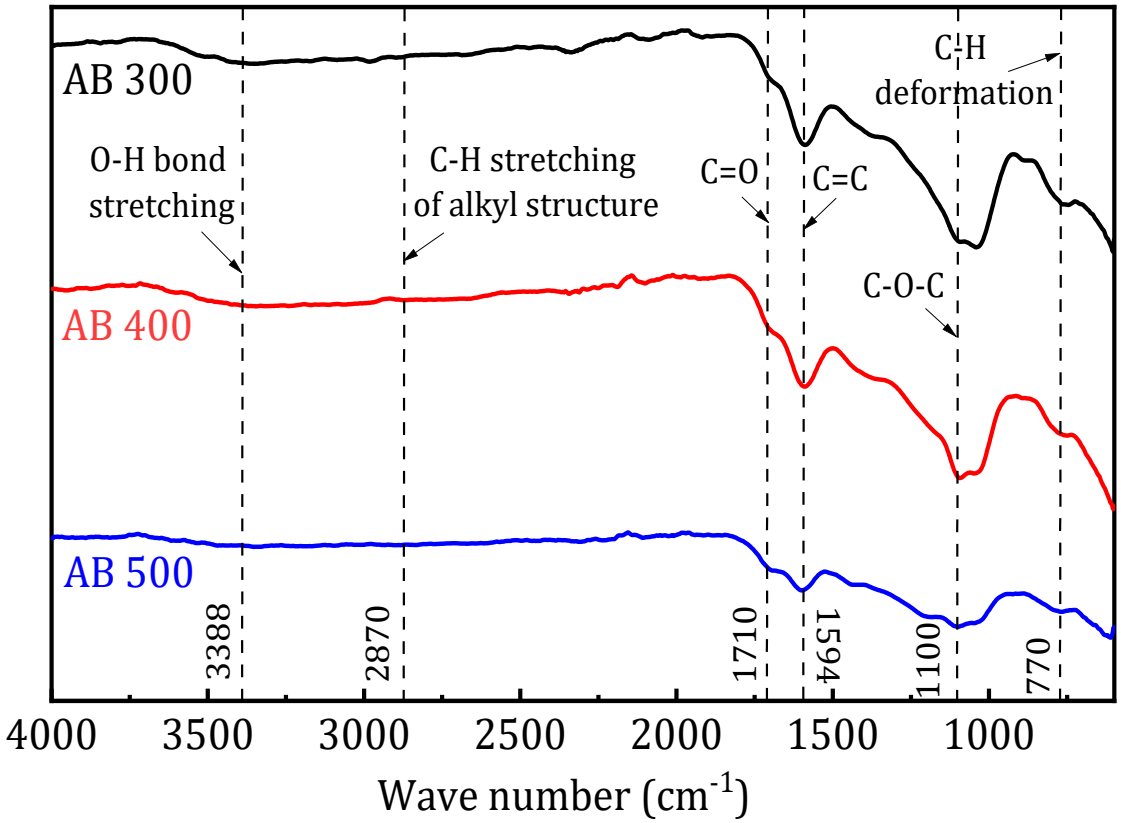

Fig. 10. FTIR Spectra of AB

The degree of crystallinity of AB samples was analyzed by studying the XRD, as shown in Fig. 11. The broad diffraction peak observed between 16-25°C is characteristic of the lignocellulose crystalline phase (Zhang et al., 2024), eliminated at higher pyrolysis temperatures. All AB samples exhibit a hump in the range of 16-25°, approximately 22°, indicating a caron-rich amorphous structure (Pariyar et al., 2020) and aliphatic chains representing aromatic carbon rings. With increasing pyrolysis temperature, the peak at 26° becomes sharper and narrower, suggesting the development of highly crystalline graphic carbon in the biochar (Kakaei et al., 2019). This observation agrees with the aromatization

development in the FTIR and TGA analysis. The XRD pattern of AB 500 reveals additional well-defined peaks at 20°, attributed to the presence of quartz (SiO_2), which agrees with the EDX of AB 500, shown in Fig. S2.

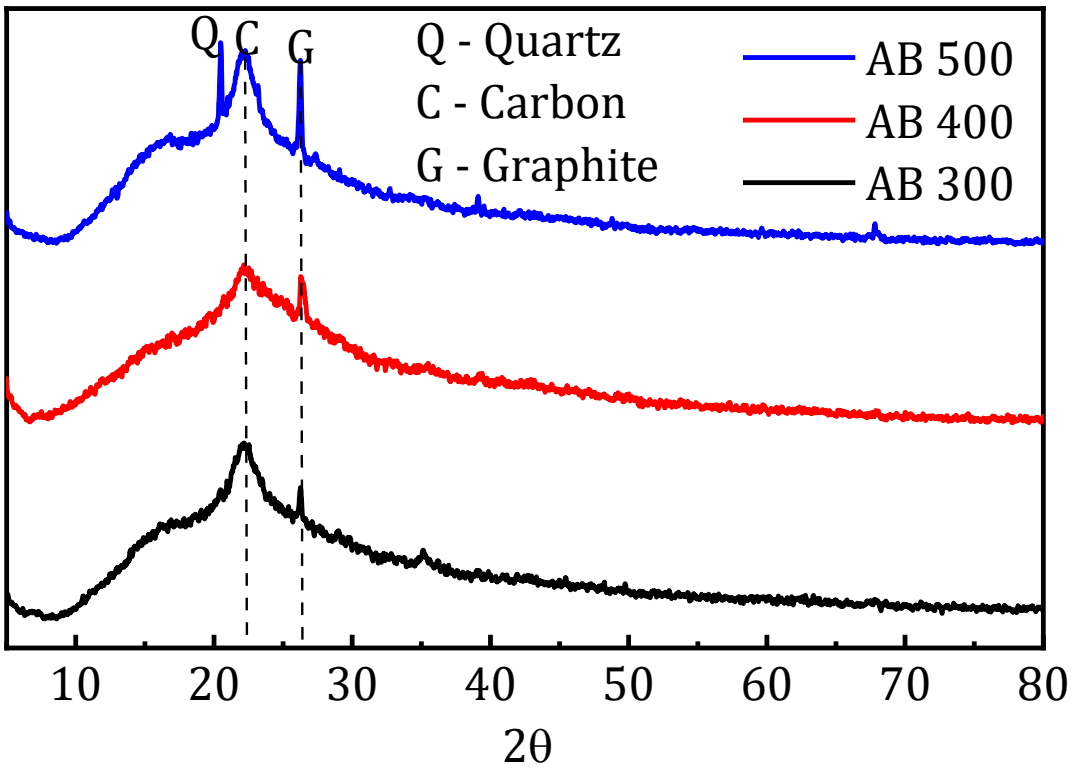

Fig. 11. XRD of AB

3.2 Effect of AB on Compressive Strength

The compressive strength of all the mortar mixes at 7 and 28 days is illustrated in Fig. 12. The addition of AB significantly affects the mechanical properties of cementitious composites. Regardless of its preparation temperature, incorporating AB into the mortar increases compressive strength compared to the control mortar (PC). As the curing age increases, all the mortar specimens consistently exhibit improved strength due to the continuous increase in the hydration products. At 7 and 28 days, the compressive strength of AB 300 increased by 8% and 12%, AB 400 increased by 16% and 21%, and AB 500 increased by 27% and 34%, respectively, with respect to the control mortar. From 7 to 28 days, the compressive strength of PC, AB 300, AB 400, and AB 500 increased by 37%, 42%, 43%, and 45%, respectively. However, an improvement was observed in the mortar prepared with AB 500 compared to AB 300 and AB 400. The reason for the improvement in strength is attributed to the micro-filler effect of AB accelerating the hydration process and the fine particles of AB, resulting in a better packing and denser matrix (Manjunath et al., 2024). Additionally, biochar's hydrophilic and porous characteristics absorb a portion of the mixing water and subsequently release it to develop an

internal curing effect (Kua, 2024). This internal curing effect facilitated the production of calcium silicate hydrate (C-S-H), a critical factor contributing to strength enhancement (Javed et al., 2022). Further, the study conducted by Goldman et al. (Goldman and Bentur, 1994) reported that incorporating micro-fillers of carbon particles has a more significant strengthening effect than the pozzolanic effect.

The two-way ANOVA was conducted to examine the effects of pyrolysis temperature and curing age on the strength of the mortar. The results are presented in Table S3. The analysis revealed that pyrolysis temperature ($F(3,19) = 34.41$, $p < 0.0001$) and curing age ($F(1,19) = 280.91$, $p < 0.0001$) have significant influence on the strength of biochar cementitious composites. The overall model also showed a considerable effect ($F(4, 19) = 96.03$, $p < 0.0001$), indicating that the combination of pyrolysis temperature and curing age significantly predicts variations in the strength of the mortar.

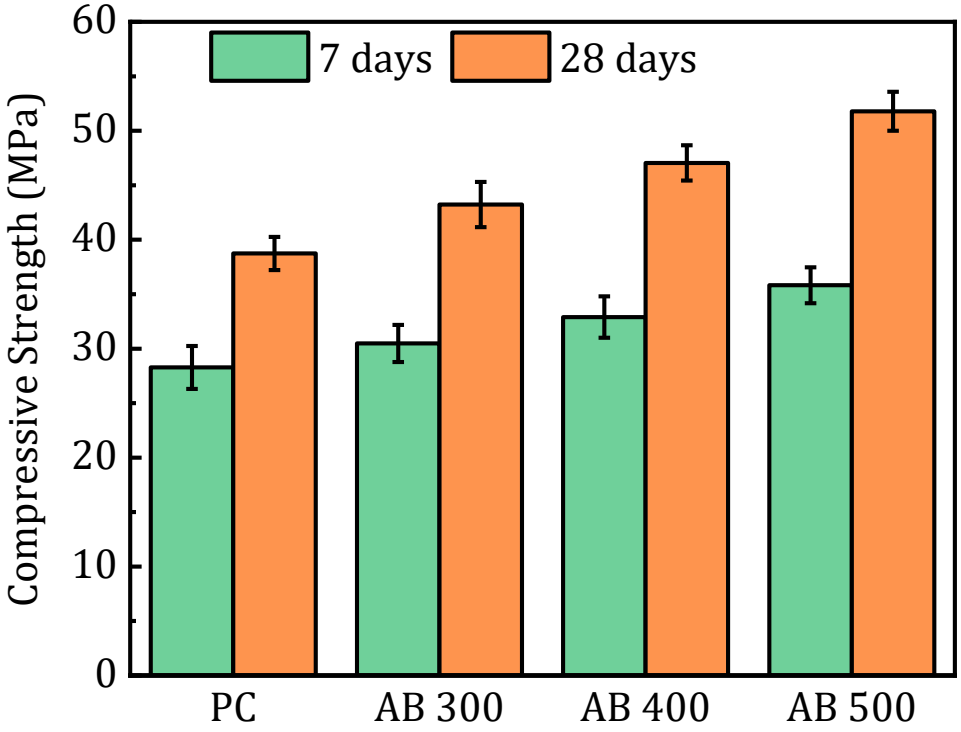

Fig. 12. Compressive strength of the AB blended mortar

3.3 Effect of AB on Ultrasonic Pulse Velocity (UPV)

The UPV is a non-destructive test used to evaluate the quality, homogeneity, and uniformity of concrete structures (Manjunath et al., 2023). It involves sending ultrasonic waves through the material and measuring the time it takes for the waves to travel from one point to another. Fig. 13 presents the UPV test results for all the mortar specimens. Similar to the increase in compressive strength, the UPV of the specimens also shows an increasing trend with age. The

UPV of specimen PC were 4214 m/s and 4456 m/s at 7 and 28 days, respectively. The UPV of AB 300, AB 400, and AB 500 at 7 and 28 days were 4421 m/s and 4625 m/s, 4512 m/s and 4708 m/s, 4630 m/s and 4810 m/s. The UPV test results for all the specimens were greater than 4200 m/s, indicating good quality. However, for biochar blended samples, the UPV results were greater than 4500 m/s at 28 days, indicating its excellent quality (Research and Feldman, 1977). Biochar particles are generally finer than the average size of cement grains, and these fine particles play a crucial role in obstructing the pores within the mortar, thereby promoting the compactness of the blended mortar (Maljaee et al., 2021a). Further, the excellent water retention capacity of AB facilitates the gradual release of the retained water during later stages, effectively serving as an internal curing agent that contributes to the densification of the matrix (Gupta et al., 2018b). Consequently, this results in a shorter transmission time for ultrasonic waves to travel, leading to an increase in wave velocity.

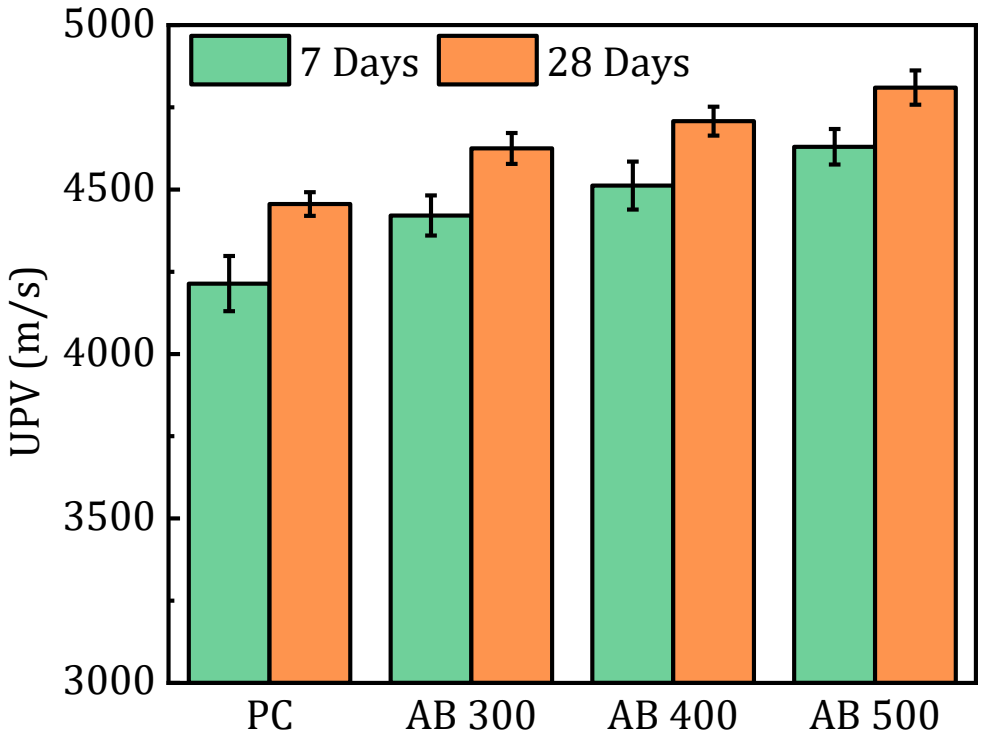

Fig. 13. UPV of the AB blended mortar

3.4 Effect of AB on cement hydration

3.4.1 Thermogravimetric analysis (TGA)

Fig. 14 (a) and Fig. 14 (b) show the TGA and DTG curves for the AB blended samples at 7 days, and the temperature ranges from 30 to 900°C. The DTG curves are divided into three major peaks; the first peak before 100°C is due to the dehydration of C-S-H, AFt, and other

hydration products. This peak increases with the addition of AB, irrespective of temperature, due to the ability of the biochar to absorb free water from the surrounding environment. The second peak in the DTG curve arises from the dehydroxylation of calcium hydroxide (CH). Except for AB 300, all other samples exhibit higher peaks. This phenomenon can be attributed to the unique hydration characteristics induced by biochar. Biochar accelerates the early-stage hydration process, resulting in the formation of more CH. The third peak corresponds to the decomposition of calcite. All the AB samples showed increased peaks compared to the control sample. The accelerated hydration due to biochar leads to higher CH concentrations, leading to an increase in the calcium carbonate (CC) during carbonation.

TGA provides valuable insights into the distribution of hydration products. The following equation was used to determine the hydration and carbonated product formation of the AB blended cement paste based on the weight loss in the TGA.

$$\% \, CH_{dx} = 4.11 \times dx_{(400-500°C)} \quad (7)$$

Where CH_{dx} and $dx_{(400–500°C)}$ are the calcium hydroxide content and loss of mass in the decarboxylation zone, respectively.

The degree of hydration (α) was determined using Bhatty's method, as outlined in the following equations.

$$W_b = W_{dh} + W_{dx} + 0.41\, W_{dc} \quad (8)$$

Where W_b = chemically bound water, W_{dh} (105 – 400°C), W_{dx} (400 – 500°C), and W_{dc} (500 – 900°C) are the weight loss caused by dehydration, de-hydroxylation, and decarbonation. The factor 0.41 is employed to convert the mass loss resulting from decarbonation into the equivalent molecular weight of water.

$$\alpha \, (\%) = W_b / 0.24 \times 100 \quad (9)$$

The value 0.24 corresponds to the theoretical maximum water needed for the complete hydration of cement particles.

The degree of hydration at 7 days was calculated based on the above equations. The AB blended samples had a comparable degree of hydration. The results from Table 6 indicated that AB blended pastes exhibited a higher degree than PC. This enhancement is attributed to the large surface area of AB particles, which facilitates additional sites for chemical reactions during hydration. Additionally, the water–retention capacity of biochar, owing to its porous structure, further contributes to increased hydration. Overall, the positive influence of AB-blended samples on cement hydration leads to improved mechanical properties. The degree of hydration is consistent with other studies (Ali et al., 2023; Dixit et al., 2019).

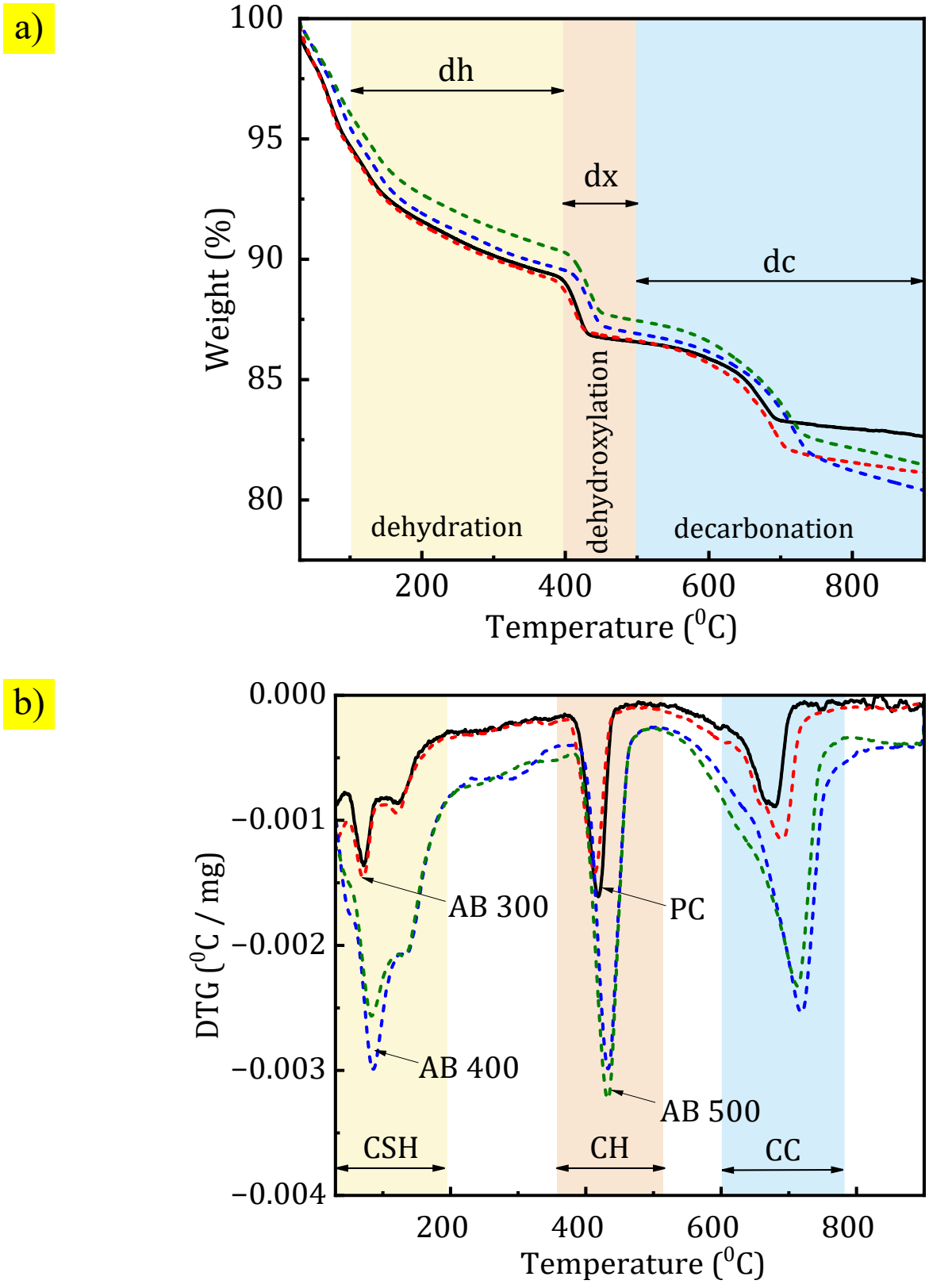

Fig. 14. TGA – DTG analysis of the blended pastes

446

447

448

449 **Table 6** Determination of hydration products using TGA analysis.

Percentage of weight loss for hydration products at various temperature ranges							
Mixes	**Biochar (%)**	**W_{dh}**	**W_{dx}**	**W_{dc}**	**W_b**	**CH (%)**	**α (%)**
PC	0%	6.13	2.82	4.74	10.92	11.68	45.50
AB 300	2%	6.44	2.35	6.75	11.56	9.68	48.19
AB 400	2%	6.35	3.02	8.09	12.70	12.43	52.92
AB 500	2%	6.14	3.23	7.36	12.40	13.30	51.68

450 **3.4.2 Fourier Transform Infrared Spectroscopy (FTIR)**

451 The FTIR analyses illustrated in Fig. 15 were used to analyze the functional groups of control,
452 and AB blended cement pastes at different pyrolysis temperatures at 7 days of curing. The
453 prominent peaks are observed at 870 cm^{-1} and 952 cm^{-1}, which is attributed to Si-O-Si bonds
454 and v_2 of CO_3^{2-} in C-S-H, respectively (Javed et al., 2022). The intensity of the peaks suggests
455 that AB promotes silicate phase hydration, leading to increased C-S-H formation. The v_2 peak
456 corresponds to the asymmetric stretching vibration of CO_3^{2-}. With the increase in pyrolysis
457 temperature, the AB contributes to the formation of carbonates during the hydration process.
458 The other peaks at 1110 cm^{-1} are associated with the stretching vibration of SO_4^{2-} ions in Aft
459 (Lin et al., 2021). The peak at 3630 cm^{-1} corresponds to the stretching vibration of OH^- in CH
460 (Ali et al., 2023). The absorption band at 1430 cm^{-1} represents the asymmetric stretching
461 vibration of CO_3^{2-} (Hughes et al., 1995). The increased peak intensity in AB blended samples
462 suggests accelerated hydration. This high degree of hydration contributes to the higher
463 compressive strength. These FTIR results are in good agreement with the observed
464 compressive strength and TGA-DTG. Incorporating AB in cement composites leads to
465 significant hydration products, potentially enhancing the overall performance of cement
466 composites.

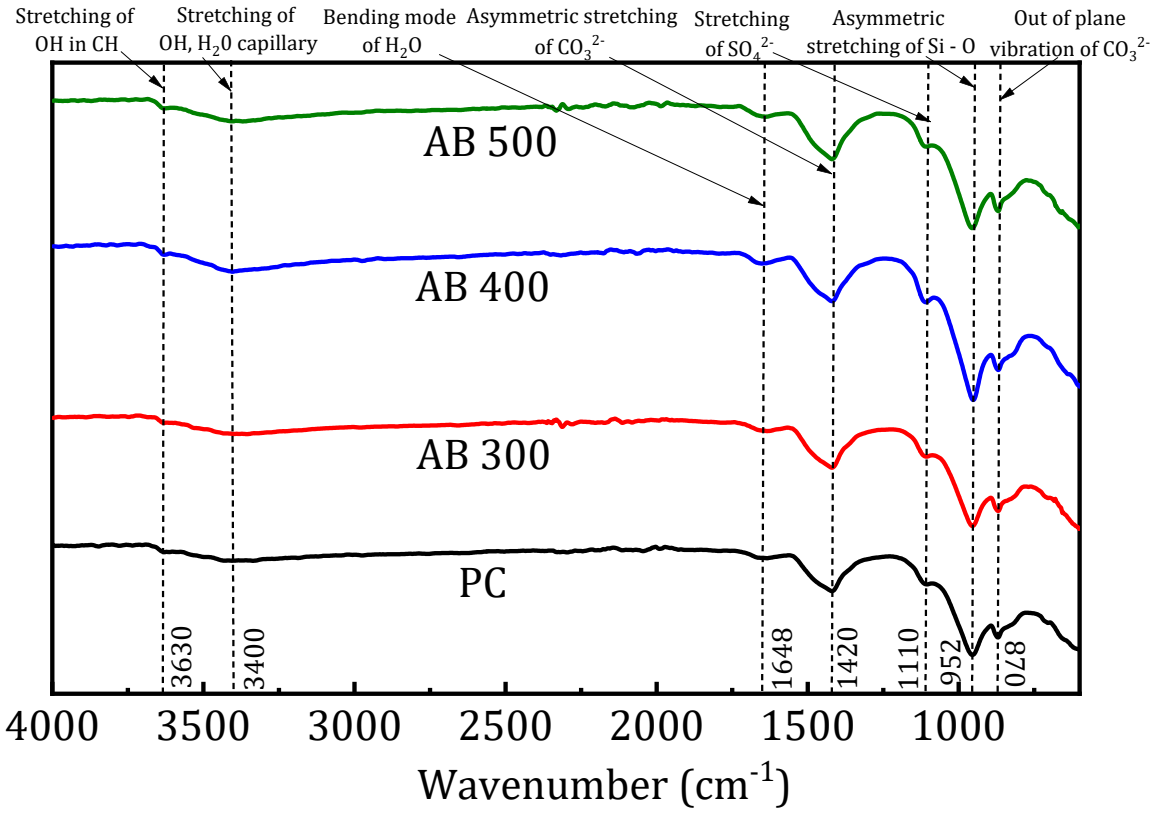

Fig. 15. FTIR analysis of the blended pastes

3.4.3 X-ray Diffraction

In the XRD results shown in Fig. 16, the cement pastes containing AB 300, AB 400, and AB 500 at 7 days exhibited distinct peaks corresponding to (P – CH (calcium hydroxide), C – CC (calcium carbonate), Q – silica, T – Alite, D- Belite (Maljaee et al., 2021b). The CH peak observed at 2Θ angles of 18°, 29.29°, 33.96°, 47.04°, 50.68°, and 62.38° increased in the AB blended samples, regardless of the pyrolysis temperature, than the control samples. These findings suggest that AB significantly accelerates the hydration process. Biochar particles act as a nucleation site for CH and other hydration products, resulting in higher CH concentration during the early stages of hydration (Qu et al., 2024; Zhu et al., 2023). Additionally, the CC peaks primarily detected at 2Θ angles of 23° and 39.3° exhibited an increasing trend in biochar blended samples. The enhanced CH content during early hydration contributes to carbonation to form CC peaks. The results from TGA further support this observation. Unlike crystalline phases, C-S-H has a gel structure crucial for cement strength and does not produce distinct peaks in XRD. Peaks at 2Θ angles 32° and 41° correspond to T and D, respectively. The peak at 26.8° in the AB 500 sample indicates the presence of Q, resulting in enhanced compressive strength. Overall, the addition of AB, regardless of the pyrolysis temperature, influences

hydration, promoting T and D phases and contributing to increased C-S-H content, which enhances overall strength development (Javed et al., 2022).

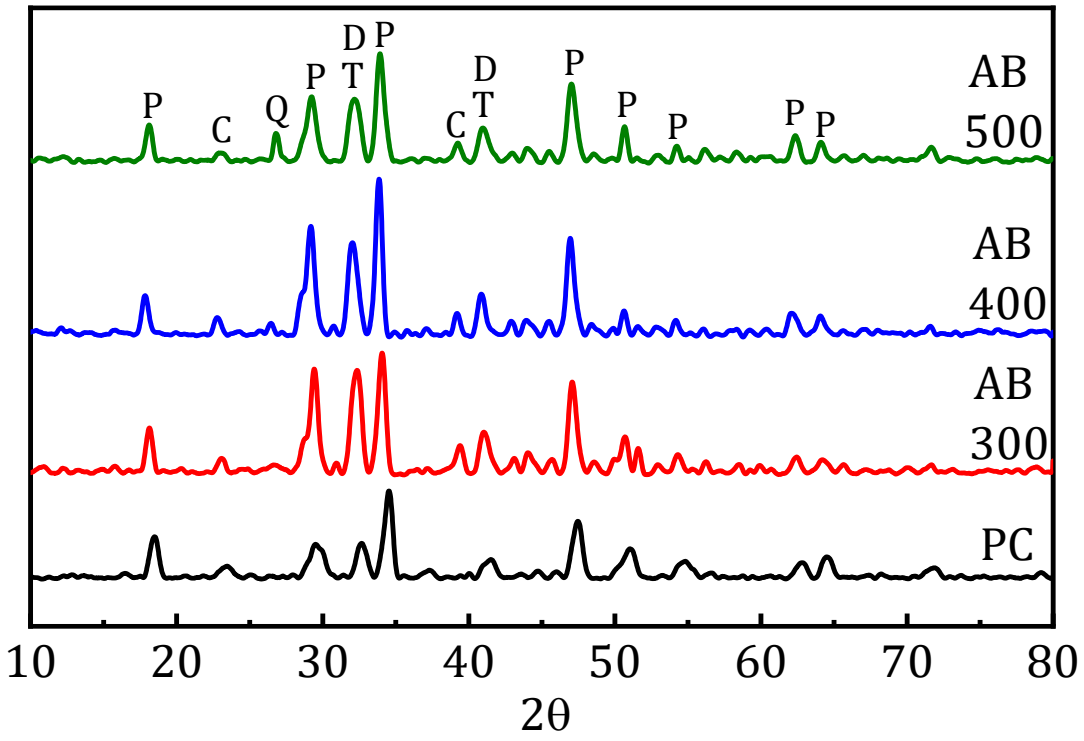

Fig. 16. XRD analysis of the blended pastes

Fig. 17 illustrates the hydration mechanism of cement and AB blended pastes. The comprehensive analysis of the effect of AB on cement hydration through TGA, FTIR, and XRD analysis findings reveals a consistent pattern of enhanced hydration reaction. The hydration process results in the formation of C-S-H and CH, creating a layer of hydration products on the cement grains (illustrated by blue circles), as shown in Fig. 17 (A). Fig. 17 (B) shows small-sized AB particles dispersed between the larger cement grains. During hydration, AB accelerates early-stage hydration and attracts positively charged hydrated cement particles around them due to its surface negative charge (Gupta et al., 2021). This forms nucleation clusters that promote the growth of hydration products on the surface, which is consistent with the TGA and XRD results showing accelerated early-stage hydration and increased CH peaks. Further, the formation of hydration products is consistent with the increased intensity observed in FTIR analysis, while XRD results show higher CH and CC in AB blended pastes. This also correlates with the improved mechanical properties and a higher degree of hydration observed in TGA for AB-blended cementitious composites. At 7 days, the hydration process results in the formation of C-S-H, CH, and CC, leading to a denser structure and enhancing the overall performance of the cement composite.

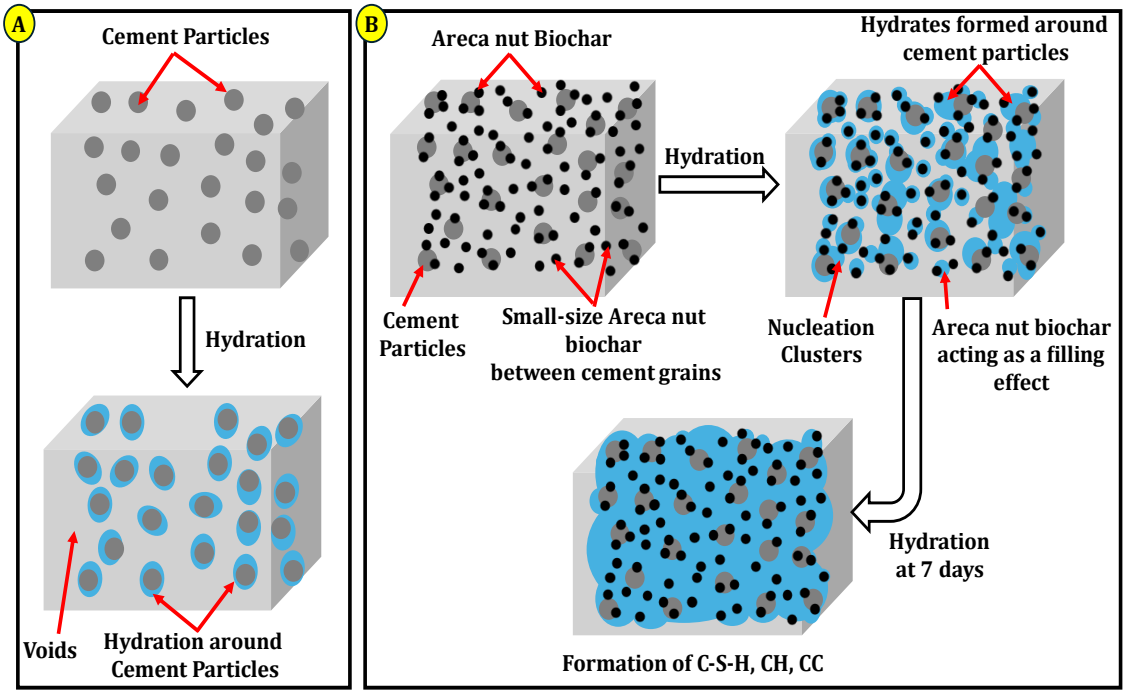

Fig. 17. Schematic diagram showing hydration product in cement and blended biochar pastes

Fig. 18 shows the SEM images of the control and AB blended paste (PC, AB 300, AB 400, and AB 500) after 7 days of curing. All the AB blended samples exhibited the formation of hydration products, needle-shaped ettringite, C-S-H, and crystals of CH (shown by yellow circles). Compared to PC, even a small amount of biochar provides additional hydration sites and creates a closer interconnection. Moreover, the particle size of the biochar enables them to act as micro-reinforcers in cement, resulting in denser structures. Biochar pores absorb water during mixing, facilitating the formation of hydration products within the structure, which contributes to the strength of the cement matrix.

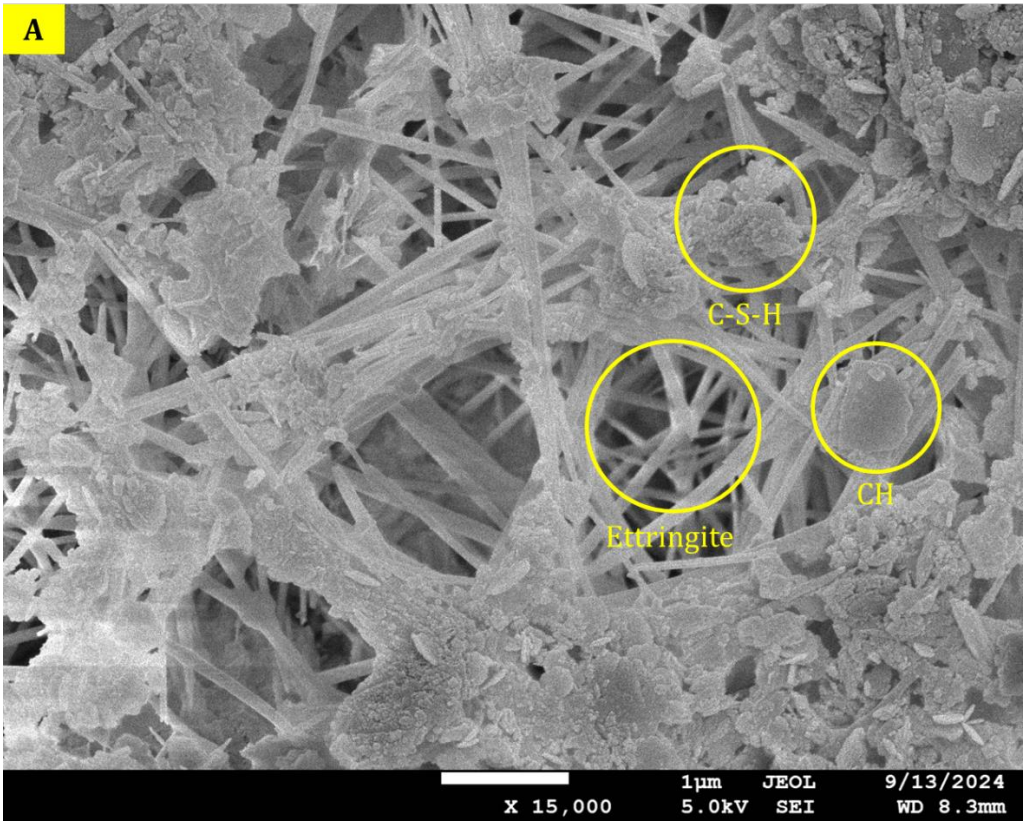
A
C-S-H
CH
Ettringite
X 15,000
1µm JEOL
5.0kV SEI
9/13/2024
WD 8.3mm

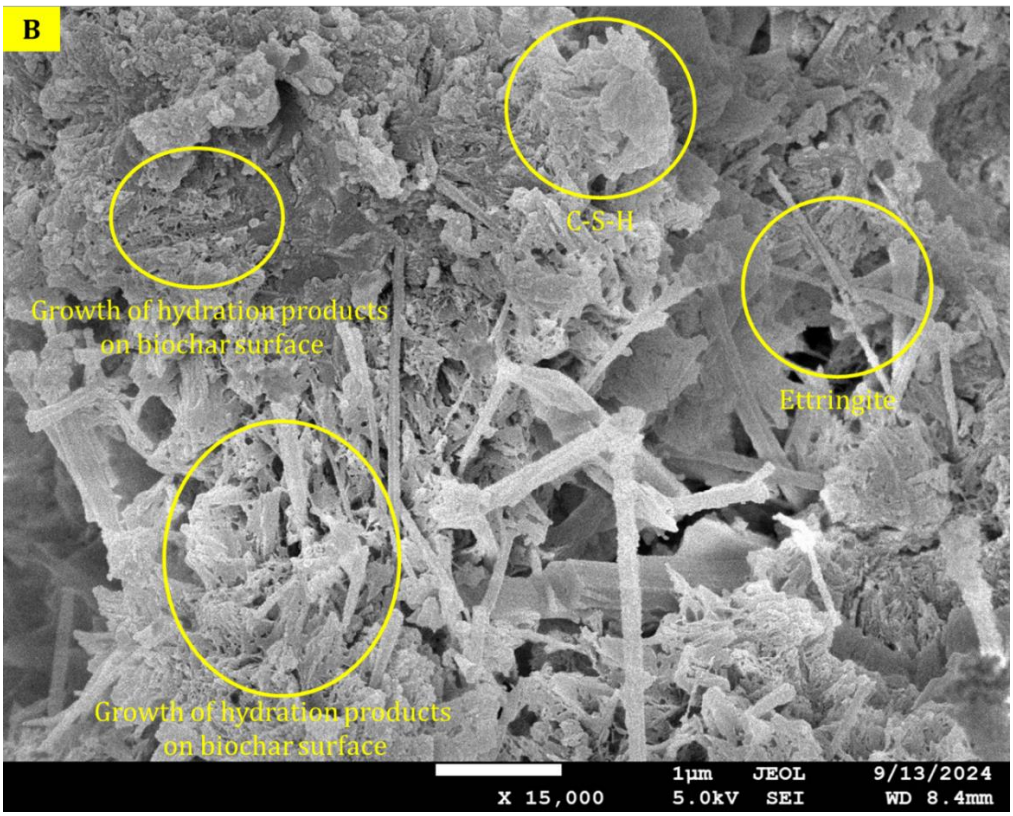
B
C-S-H
Growth of hydration products on biochar surface
Ettringite
Growth of hydration products on biochar surface
X 15,000
1µm JEOL
5.0kV SEI
9/13/2024
WD 8.4mm

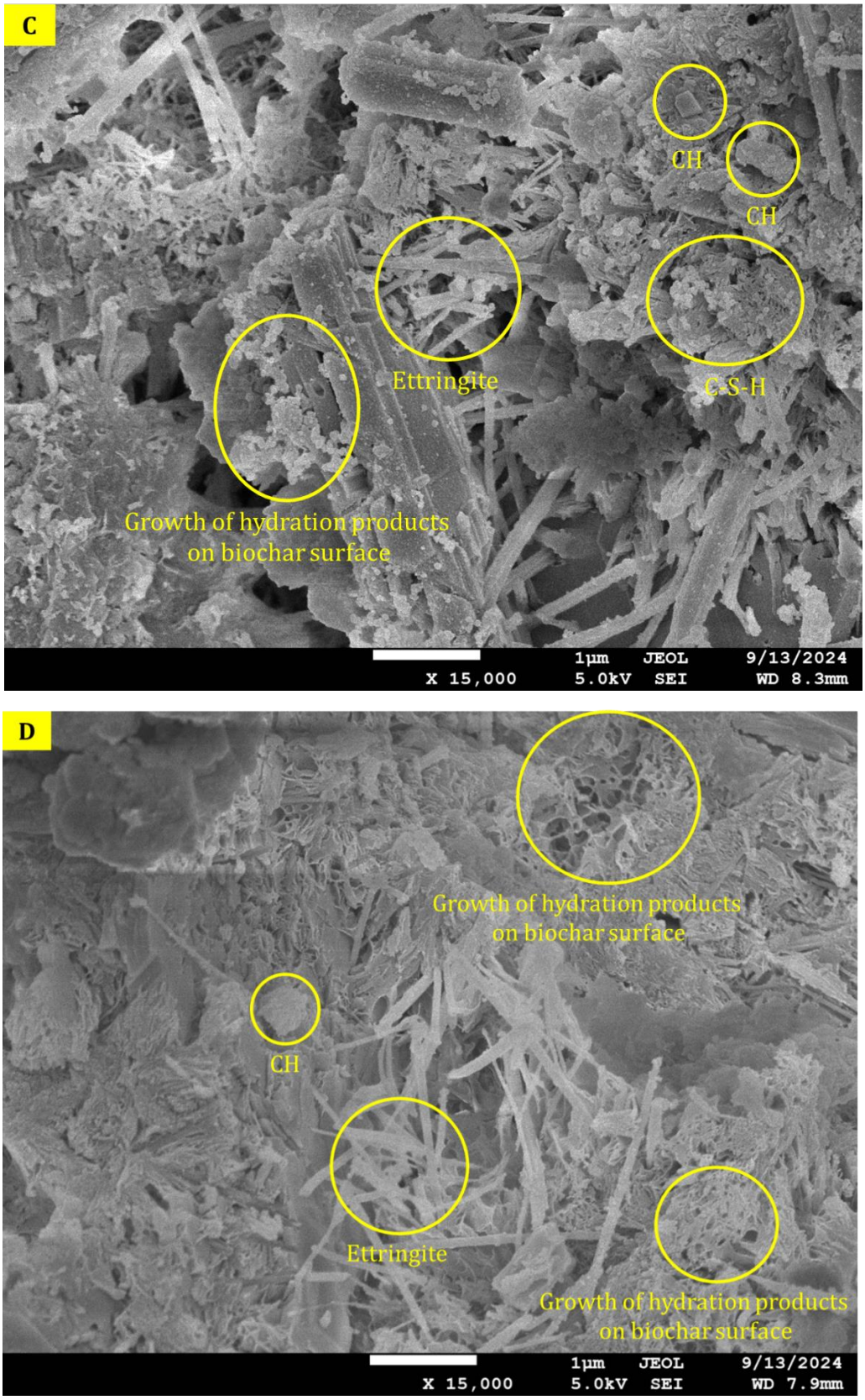

509 **Fig. 18.** SEM image of cement and blended biochar paste A) PC B) AB 300 C) AB 400 D)
510 AB 500
511

4. Environmental Benefits

The environmental benefits of incorporating AB as a carbonaceous filler to cement can be measured by the net reduction in carbon equivalent emissions related to AB blended mortars with the control mortar mixes. Table 7 presents the CO_2 equivalent values associated with the materials used. The CO_2 equivalent attributed to AB can be determined by calculating the percentage of carbon sequestered within the AB while accounting for CO_2 equivalent emissions generated during the pyrolysis. CO_2 equivalent emissions from sand and water are the same throughout the mixes. Hence, it is neglected from the calculations.

Table 7. CO_2 equivalent emissions of the materials used

Material	CO_2 equivalent ($kgCO_2/kg$)
Cement	1.002 (Grant, 2015)
AB 500	-1.771*

By considering AB 500, the carbon content in the produced AB at 500°C is 85.12% (or 851.2 per kg). 1 kg of AB 500 would lead to CO_2 sequestration of, $(44/12) \times 851.2 \approx 3121$ g or 3.121 $kgCO_2/kg$. The ratio of (44/12) is used because CO_2 has a molecular weight of 44, while C has an atomic weight of 12. Slow pyrolysis at 450 – 500°C emits 0.407 kg CO_2/kg of dry feedstock of switchgrass (Gupta and Kashani, 2021; Roberts et al., 2010). This value was used as an approximation, considering switchgrass and areca nut husk as agricultural residues. Yield of AB 500 ≈ 32% (meaning 1 kg biochar requires 3.125 kg feedstock). The emissions calculation is $3.125 \times 0.407 \approx 1.35$ $kgCO_2/kg$. Net CO2 avoidance is $(3.121 - 1.35) \approx 1.771$ $kgCO_2/kg$. The net CO_2 avoidance is $1.771 \times 0.32 \times 1000 \approx 566.72$ kg CO_2 equivalent of emission per ton of dry feedstock. The value accounts for both the CO_2 sequestered by the AB 500 and the emissions produced during the pyrolysis process.

* for every kg of AB 500 produced, there is a net reduction of 1.771 kg of CO_2 in the atmosphere.

Table 8 illustrates the CO_2 equivalent for the control and AB 500 blended mortar mixes for a weight of 1 kg of material.

Table 8. CO_2 equivalent for the AB blended mixes

Mixes	Cement (kg)	AB (kg)	CO_2 equivalent ($kgCO_2/kg$)
PC	1.00	0	1.002
AB 500	0.92	0.08	0.780

It can be observed from Table 7 that the addition of AB 500 at 2% reduces the CO_2 equivalent by 22%. However, it is observed that the CO_2 equivalent of biochar varies depending on the feedstock, yield, carbon content, and dosage. To maximize the potential of carbon sequestration and sustainability in the construction sector, prioritizing the utilization of locally available wastes for biochar production offers environmental and economic benefits. This approach significantly reduces transportation-related emissions, minimizes waste sent to landfills, and decreases energy consumption associated with material processing. By promoting a circular economy, it transforms local waste into valuable resources, stimulating local economies and reducing dependence on imported materials. This localized strategy minimizes the carbon footprint of both biochar production and construction processes and enhances the net positive impact on carbon sequestration and overall sustainability.

5. Conclusions

This study presents an innovative approach for converting waste areca nut husk into biochar as a novel carbonaceous filler for cement. The conclusions of the findings are outlined below.

- The pyrolysis temperature has a significant influence on the characteristics of AB. Higher temperatures accelerate carbonization and promote the formation of aromatic carbon structure.
- The AB blended cement mortars showed higher compressive strength than the control mortar at 7 and 28 days. The micro-filler effect and porous nature of AB accelerate the hydration process by absorbing a portion of the mixing water and subsequently releasing it, thereby enhancing the compressive strength.
- TGA, FTIR, XRD, and SEM analysis confirmed increased hydration product formation in AB cement pastes. Furthermore, the degree of hydration from Bhatty's method increased with the addition of AB.
- The partial replacement of cement with AB effectively reduces CO2 equivalent emissions in cement mortar production through decreased cement consumption and the negative carbon footprint of AB.

AB offers a sustainable solution as a novel carbonaceous filler, enhancing strength and hydration in cement composites. The findings from this study will provide a foundation for further research to optimize the performance of AB and its benefits in engineering applications. Finally, locally available agrowaste for biochar production presents an attractive option for the future of the construction industry.

Credit authorship contribution statement

Balasubramanya Manjunath: Conceptualization, Investigation, Data curation, Validation, Formal analysis, Methodology, Visualization, Writing - original draft, Writing - review & editing, Funding acquisition. **Claudiane M. Ouellet-Plamondon:** Conceptualization, Data curation, Validation, Writing - review & editing. **B.B. Das:** Data curation, Validation, Writing - review & editing. **Subba Rao:** Data curation, Validation, Writing - review & editing. **Chandrasekhar Bhojaraju:** Conceptualization, Investigation, Data curation, Validation, Formal analysis, Methodology, Visualization, Supervision, Writing – review & editing. **Manu Rao:** Conceptualization, Investigation, Data curation, Validation, Formal analysis, Methodology, Visualization, Supervision, Writing – review & editing.

Declaration of competing interest

The authors declare that they have no known competing financial interests or personal relationships that could have appeared to influence the work reported in this paper.

Data availability

No data was used for the research described in the article.

Acknowledgments

The authors thank the National Institute of Technology, Surathkal, Mangaluru, Karnataka, and St Joseph Engineering College, Mangaluru, Karnataka, for their unwavering support during this research. The authors thank the technical staff and students for supporting our experiments. The authors acknowledge the Central Research Facility and Sustainable Construction and Building Materials Laboratory of the National Institute of Technology, Surathkal, Mangaluru, Karnataka, for all the required facilities for the study.

Funding sources

This work was supported by the St Joseph Engineering College - Seed money grant [Grant Number: SJEC/Prin/OC/2023/047]

References

Akhtar, A., Sarmah, A.K., 2018. Novel biochar-concrete composites: Manufacturing, characterization and evaluation of the mechanical properties. Science of the total environment 616, 408-416.

Ali, D., Agarwal, R., Hanifa, M., Rawat, P., Paswan, R., Rai, D., Tyagi, I., Naik, B.S., Pippal, A., 2023. Thermo-physical properties and microstructural behaviour of biochar-incorporated cementitious material. Journal of Building Engineering 64, 105695.

Andrew, R.M., 2018. Global CO 2 emissions from cement production. Earth System Science Data 10, 195-217.

Anuar, M.F., Fen, Y.W., Azizan, M.Z., Rahmat, F.i., Zaid, M.H.M., Khaidir, R.E.M., Omar, N.A.S., 2021. Sustainable production of arecanut husk ash as potential silica replacement for synthesis of silicate-based glass-ceramics materials. Materials 14, 1141.
Azzi, E.S., Karltun, E., Sundberg, C., 2019. Prospective life cycle assessment of large-scale biochar production and use for negative emissions in Stockholm. Environmental science & technology 53, 8466-8476.
Bardalai, M., Mahanta, D., 2018. Characterisation of biochar produced by pyrolysis from areca catechu dust. Materials Today: Proceedings 5, 2089-2097.
Bera, S., Mohanty, K., 2020. Areca nut (Areca catechu) husks and Luffa (Luffa cylindrica) sponge as microbial immobilization matrices for efficient phenol degradation. Journal of Water Process Engineering 33, 100999.
Bhojaraju, C., Di Mare, M., Ouellet-Plamondon, C.M., 2021. The impact of carbon-based nanomaterial additions on the hydration reactions and kinetics of GGBS-modified cements. Construction and Building Materials 303, 124366.
Cantrell, K.B., Hunt, P.G., Uchimiya, M., Novak, J.M., Ro, K.S., 2012. Impact of pyrolysis temperature and manure source on physicochemical characteristics of biochar. Bioresource technology 107, 419-428.
Chen, X., Lin, B., 2021. Towards carbon neutrality by implementing carbon emissions trading scheme: Policy evaluation in China. Energy Policy 157, 112510.
DHNS, 2020. Indiscriminate dumping of arecanut husk worries residents. Deccan Herald, Karnataka.
Dixit, A., Gupta, S., Dai Pang, S., Kua, H.W., 2019. Waste Valorisation using biochar for cement replacement and internal curing in ultra-high performance concrete. Journal of Cleaner Production 238, 117876.
Dixit, A., Verma, A., Dai Pang, S., 2021. Dual waste utilization in ultra-high performance concrete using biochar and marine clay. Cement and Concrete Composites 120, 104049.
Elnour, A.Y., Alghyamah, A.A., Shaikh, H.M., Poulose, A.M., Al-Zahrani, S.M., Anis, A., Al-Wabel, M.I., 2019. Effect of pyrolysis temperature on biochar microstructural evolution, physicochemical characteristics, and its influence on biochar/polypropylene composites. Applied sciences 9, 1149.
Gogoi, D., Bordoloi, N., Goswami, R., Narzari, R., Saikia, R., Sut, D., Gogoi, L., Kataki, R., 2017. Effect of torrefaction on yield and quality of pyrolytic products of arecanut husk: An agro-processing wastes. Bioresource technology 242, 36-44.
Goldman, A., Bentur, A., 1994. Properties of cementitious systems containing silica fume or nonreactive microfillers. Advanced Cement Based Materials 1, 209-215.
Grant, T., 2015. Life cycle inventory of cement & concrete produced in Australia. Melbourne, Australia.
Gujre, N., Mitra, S., Agnihotri, R., Sharma, M.P., Gupta, D., 2022. Novel agrotechnological intervention for soil amendment through areca nut husk biochar in conjunction with vetiver grass. Chemosphere 287, 132443.
Gupta, S., Kashani, A., 2021. Utilization of biochar from unwashed peanut shell in cementitious building materials–Effect on early age properties and environmental benefits. Fuel Processing Technology 218, 106841.
Gupta, S., Kua, H.W., 2018. Effect of water entrainment by pre-soaked biochar particles on strength and permeability of cement mortar. Construction and Building Materials 159, 107-125.
Gupta, S., Kua, H.W., Dai Pang, S., 2018a. Biochar-mortar composite: Manufacturing, evaluation of physical properties and economic viability. Construction and Building Materials 167, 874-889.
Gupta, S., Kua, H.W., Koh, H.J., 2018b. Application of biochar from food and wood waste as green admixture for cement mortar. Science of the total environment 619, 419-435.
Gupta, S., Kua, H.W., Low, C.Y., 2018c. Use of biochar as carbon sequestering additive in cement mortar. Cement and concrete composites 87, 110-129.
Gupta, S., Muthukrishnan, S., Kua, H.W., 2021. Comparing influence of inert biochar and silica rich biochar on cement mortar–Hydration kinetics and durability under chloride and sulfate environment. Construction and Building Materials 268, 121142.

Habert, G., Miller, S.A., John, V.M., Provis, J.L., Favier, A., Horvath, A., Scrivener, K.L., 2020. Environmental impacts and decarbonization strategies in the cement and concrete industries. Nature Reviews Earth & Environment 1, 559-573.
Hugar, P., Dutta, A., Srilakshmi, S., Belur, P.D., Raval, K., Iyyaswami, R., 2023. Phenolic profile of unripe areca nuts cultivated in various districts of Karnataka, India. JSFA Reports.
Hughes, T.L., Methven, C.M., Jones, T.G., Pelham, S.E., Fletcher, P., Hall, C., 1995. Determining cement composition by Fourier transform infrared spectroscopy. Advanced Cement Based Materials 2, 91-104.
Javed, M.H., Sikandar, M.A., Ahmad, W., Bashir, M.T., Alrowais, R., Wadud, M.B., 2022. Effect of various biochars on physical, mechanical, and microstructural characteristics of cement pastes and mortars. Journal of Building Engineering 57, 104850.
Kakaei, K., Esrafili, M.D., Ehsani, A., 2019. Characterization, Interface science and technology. Elsevier, pp. 109-151.
Kalderis, D., Anastasiou, E., Petrakis, E., Konopisi, S., 2024. Utilization of biochar from olive tree pruning as additive to cement mortars. Journal of Cleaner Production 469, 143137.
Karić, N., Maia, A.S., Teodorović, A., Atanasova, N., Langergraber, G., Crini, G., Ribeiro, A.R., Đolić, M., 2022. Bio-waste valorisation: Agricultural wastes as biosorbents for removal of (in) organic pollutants in wastewater treatment. Chemical Engineering Journal Advances 9, 100239.
Khan, H.M., Iqbal, T., Yasin, S., Ali, C.H., Abbas, M.M., Jamil, M.A., Hussain, A., M. Soudagar, M.E., Rahman, M.M., 2021. Application of agricultural waste as heterogeneous catalysts for biodiesel production. Catalysts 11, 1215.
Kim, C., Talapaneni, S.N., Dai, L., 2023. Porous carbon materials for CO2 capture, storage and electrochemical conversion. Materials Reports: Energy 3, 100199.
Kloss, S., Zehetner, F., Dellantonio, A., Hamid, R., Ottner, F., Liedtke, V., Schwanninger, M., Gerzabek, M.H., Soja, G., 2012. Characterization of slow pyrolysis biochars: effects of feedstocks and pyrolysis temperature on biochar properties. Journal of environmental quality 41, 990-1000.
Kua, H., Tan, S., 2023. Novel typology of accelerated carbonation curing: using dry and pre-soaked biochar to tune carbon capture and mechanical properties of cementitious mortar. Biochar 5, 36.
Kua, H.W., 2024. Biochar as building and road materials, Biochar for Environmental Management. Routledge, pp. 719-733.
Lee, K.-T., Chen, W.-H., Sarles, P., Park, Y.-K., Ok, Y.S., 2022. Recover energy and materials from agricultural waste via thermalchemical conversion. One Earth 5, 1200-1204.
Lehmann, J., Rillig, M.C., Thies, J., Masiello, C.A., Hockaday, W.C., Crowley, D., 2011. Biochar effects on soil biota–a review. Soil biology and biochemistry 43, 1812-1836.
Li, S., Chen, G., 2018. Thermogravimetric, thermochemical, and infrared spectral characterization of feedstocks and biochar derived at different pyrolysis temperatures. Waste Management 78, 198-207.
Lin, R.-S., Lee, H.-S., Han, Y., Wang, X.-Y., 2021. Experimental studies on hydration–strength–durability of limestone-cement-calcined Hwangtoh clay ternary composite. Construction and Building Materials 269, 121290.
Liu, C., Yao, Z., Wang, K., Zheng, X., Li, B., 2019. Net ecosystem carbon and greenhouse gas budgets in fiber and cereal cropping systems. Science of the Total Environment 647, 895-904.
Maljaee, H., Madadi, R., Paiva, H., Tarelho, L., Ferreira, V.M., 2021a. Incorporation of biochar in cementitious materials: A roadmap of biochar selection. Construction and Building Materials 283, 122757.
Maljaee, H., Paiva, H., Madadi, R., Tarelho, L.A., Morais, M., Ferreira, V.M., 2021b. Effect of cement partial substitution by waste-based biochar in mortars properties. Construction and Building Materials 301, 124074.
Manjunath, B., Ouellet-Plamondon, C.M., Das, B., Bhojaraju, C., 2023. Potential utilization of regional cashew nutshell ash wastes as a cementitious replacement on the performance and environmental impact of eco-friendly mortar. Journal of Building Engineering 66, 105941.
Manjunath, B., Ouellet-Plamondon, C.M., Ganesh, A., Das, B., Bhojaraju, C., 2024. Valorization of coffee cherry waste ash as a sustainable construction material. Journal of Building Engineering, 110796.

Marescaux, A., Thieu, V., Garnier, J., 2018. Carbon dioxide, methane and nitrous oxide emissions from the human-impacted Seine watershed in France. Science of the Total Environment 643, 247-259.
Ollivier, S., Jéhan, P., Olivier-Jimenez, D., Lambert, F., Boustie, J., Lohézic-Le Dévéhat, F., Le Yondre, N., 2022. New insights into the Van Krevelen diagram: Automated molecular formula determination from HRMS for a large chemical profiling of lichen extracts. Phytochemical Analysis 33, 1111-1120.
Pariyar, P., Kumari, K., Jain, M.K., Jadhao, P.S., 2020. Evaluation of change in biochar properties derived from different feedstock and pyrolysis temperature for environmental and agricultural application. Science of the Total Environment 713, 136433.
Patwa, D., Bordoloi, U., Dubey, A.A., Ravi, K., Sekharan, S., Kalita, P., 2022. Energy-efficient biochar production for thermal backfill applications. Science of The Total Environment 833, 155253.
Qu, F., Zhang, Y., Zhu, X., Xu, W., Poon, C.S., Li, W., Tsang, D.C., 2024. Roles of wood waste biochar for chloride immobilization in GGBS-blended cement composites. Construction and Building Materials 411, 134389.
Rafiq, M.K., Bachmann, R.T., Rafiq, M.T., Shang, Z., Joseph, S., Long, R., 2016. Influence of pyrolysis temperature on physico-chemical properties of corn stover (Zea mays L.) biochar and feasibility for carbon capture and energy balance. PloS one 11, e0156894.
Rashid, S., Raghav, A., Goyal, A., AB, D.R., Singh, M., 2024. Biochar as a sustainable additive in cementitious composites: A comprehensive analysis of properties and environmental impact. Industrial Crops and Products 209, 118044.
Research, N.R.C.o.C.D.o.B., Feldman, R., 1977. Non-destructive testing of concrete.
Reza, M.S., Afroze, S., Bakar, M.S., Saidur, R., Aslfattahi, N., Taweekun, J., Azad, A.K., 2020. Biochar characterization of invasive Pennisetum purpureum grass: effect of pyrolysis temperature. Biochar 2, 239-251.
Roberts, K.G., Gloy, B.A., Joseph, S., Scott, N.R., Lehmann, J., 2010. Life cycle assessment of biochar systems: estimating the energetic, economic, and climate change potential. Environmental science & technology 44, 827-833.
Ross, A., Jones, J., Kubacki, M., Bridgeman, T., 2008. Classification of macroalgae as fuel and its thermochemical behaviour. Bioresource technology 99, 6494-6504.
Selvakumar, P., Adane, A., Zelalem, T., Hunegnaw, B., Karthik, V., Kavitha, S., Jayakumar, M., Karmegam, N., Govarthanan, M., Kim, W., 2022. Optimization of binary acids pretreatment of corncob biomass for enhanced recovery of cellulose to produce bioethanol. Fuel 321, 124060.
Sharma, R.K., Wooten, J.B., Baliga, V.L., Lin, X., Chan, W.G., Hajaligol, M.R., 2004. Characterization of chars from pyrolysis of lignin. Fuel 83, 1469-1482.
Singh, B., Dolk, M.M., Shen, Q., Camps-Arbestain, M., 2017. Biochar pH, electrical conductivity and liming potential. Biochar: A guide to analytical methods 23.
Sirico, A., Bernardi, P., Sciancalepore, C., Vecchi, F., Malcevschi, A., Belletti, B., Milanese, D., 2021. Biochar from wood waste as additive for structural concrete. Construction and Building Materials 303, 124500.
Sisman, M., Teomete, E., Yanik, J., Malayoglu, U., 2024. The effect of nano-biochar produced from various raw materials on flow and mechanical properties of mortar. Construction and Building Materials 416, 135040.
Tan, K., Pang, X., Qin, Y., Wang, J., 2020a. Properties of cement mortar containing pulverized biochar pyrolyzed at different temperatures. Construction and Building Materials 263, 120616.
Tan, Z., Yuan, S., Hong, M., Zhang, L., Huang, Q., 2020b. Mechanism of negative surface charge formation on biochar and its effect on the fixation of soil Cd. Journal of hazardous materials 384, 121370.
Thakur, D., Ramawat, N., Shyam, V., 2020. Agricultural Waste Produce: Utilization and Management. Sustainable Food Waste Management: Concepts and Innovations, 227-240.
Vikraman, V.K., Subramanian, P., Kumar, D.P., Sriramajayam, S., Mahendiran, R., Ganapathy, S., 2022. Air flowrate and particle size effect on gasification of arecanut husk with preheated air through waste heat recovery from syngas. Bioresource Technology Reports 17, 100977.

Wang, D., Zhang, W., Hao, X., Zhou, D., 2013. Transport of biochar particles in saturated granular media: effects of pyrolysis temperature and particle size. Environmental science & technology 47, 821-828.
Yang, X., Wang, X.-Y., 2021. Strength and durability improvements of biochar-blended mortar or paste using accelerated carbonation curing. Journal of CO2 Utilization 54, 101766.
Yu, S., Wang, L., Li, Q., Zhang, Y., Zhou, H., 2022. Sustainable carbon materials from the pyrolysis of lignocellulosic biomass. Materials Today Sustainability 19, 100209.
Yuan, H., Lu, T., Huang, H., Zhao, D., Kobayashi, N., Chen, Y., 2015. Influence of pyrolysis temperature on physical and chemical properties of biochar made from sewage sludge. Journal of Analytical and Applied Pyrolysis 112, 284-289.
Zeidabadi, Z.A., Bakhtiari, S., Abbaslou, H., Ghanizadeh, A.R., 2018. Synthesis, characterization and evaluation of biochar from agricultural waste biomass for use in building materials. Construction and Building Materials 181, 301-308.
Zhang, L., Yao, Z., Zhao, L., Yu, F., Li, Z., Yi, W., Fu, P., Jia, J., Zhao, Y., 2024. Effects of various pyrolysis temperatures on the physicochemical characteristics of crop straw-derived biochars and their application in tar reforming. Catalysis Today, 114663.
Zhang, Q., Li, K., Fang, Y., Guo, Z., Wei, Y., Sheng, K., 2022. Conversion from bamboo waste derived biochar to cleaner composites: Synergistic effects of aramid fiber and silica. Journal of Cleaner Production 347, 131336.
Zhang, Q., Zhang, D., Xu, H., Lu, W., Ren, X., Cai, H., Lei, H., Huo, E., Zhao, Y., Qian, M., 2020. Biochar filled high-density polyethylene composites with excellent properties: Towards maximizing the utilization of agricultural wastes. Industrial crops and products 146, 112185.
Zhu, X., Zhang, Y., Chen, L., Wang, L., Ma, B., Li, J., Poon, C.S., Tsang, D.C., 2023. Bonding mechanisms and micro-mechanical properties of the interfacial transition zone (ITZ) between biochar and paste in carbon-sink cement-based composites. Cement and Concrete Composites 139, 105004.